CONTROL OF A SATELLITE WITH FLEXIBLE SMART BEAM DURING SLEW MANEUVER

A THESIS SUBMITTED TO
THE GRADUATE SCHOOL OF NATURAL AND APPLIED SCIENCES
OF
THE MIDDLE EAST TECHNICAL UNIVERSITY

BY

HALİME ÜREK

IN PARTIAL FULFILLMENT OF THE REQUIREMENTS
FOR
THE DEGREE OF MASTER OF SCIENCE
IN
AEROSPACE ENGINEERING

SEPTEMBER 2011

Approval of the thesis:

CONTROL OF A SATELLITE WITH FLEXIBLE SMART BEAM DURING SLEW MANEUVER

submitted by **HALİME ÜREK** in partial fulfillment of the requirements for the degree of **Master of Science in Aerospace Engineering Department, Middle East Technical University** by,

Prof. Dr. Canan Özgen
Dean, Graduate School of **Natural and Applied Sciences** _____

Prof. Dr. Ozan Tekinalp
Head of Department, **Aerospace Engineering** _____

Prof. Dr. Ozan Tekinalp
Supervisor, **Aerospace Engineering Dept., METU** _____

Examining Committee Members:

Prof. Dr. Ozan Tekinalp
Aerospace Engineering Dept., METU _____

Asst. Prof. Dr. Ali Türker Kutay
Aerospace Engineering Dept., METU _____

Asst. Prof. Dr. Demirkan Çöker
Aerospace Engineering Dept., METU _____

Asst. Prof. Dr. Ercan Gürses
Aerospace Engineering Dept., METU _____

Asst. Prof. Dr. Yiğit Yazıcıoğlu
Mechanical Engineering Dept., METU _____

Date: _____

I hereby declare that all information in this document has been obtained and presented in accordance with academic rules and ethical conduct. I also declare that, as required by these rules and conduct, I have fully cited and referenced all material and results that are not original to this work.

Name, Last name : HALİME ÜREK

Signature :

ABSTRACT

CONTROL OF A SATELLITE WITH FLEXIBLE SMART BEAM DURING SLEW MANEUVER

Ürek, Halime

M.Sc. Department of Aerospace Engineering

Supervisor: Prof. Dr. Ozan Tekinalp

September 2011, 60 pages

In this thesis, an attitude control system based on Linear Quadratic Regulator (LQR) technique is developed for a hypothetical Earth observation satellite with a long flexible boom. To improve pointing performance of the satellite, the piezoelectric actuators are used as well. The boom is rectangular made of aluminum with the surface bonded piezoelectric layers on all four surfaces. The boom is modeled using finite elements. The pointing performance of the satellite using various metrics is evaluated through simulations. Effectiveness of the piezoelectric actuators is demonstrated.

Keywords: Active Control System, Active Vibration Control System, Piezoelectricity, Piezoelectric Materials, Flexible Intelligent Beam Structures, Satellite Jitter.

ÖZ

UYDUNUN YÖNELİM MANEVRASI SIRASINDA ESNEK AKILLI KİRİŞ İLE KONTROLÜ

Ürek, Halime

Yüksek Lisans, Havacılık ve Uzay Mühendisliği Bölümü

Tez Yöneticisi: Prof. Dr. Ozan Tekinalp

Eylül 2011, 60 sayfa

Bu tezde, uzun esnek bir anten kolu olan hayali bir yer gözlem uydusu için LQR kontrol tekniğine dayanan bir yönelim kontrol sistemi geliştirilmiştir. Uydunun yönelim başarımını geliştirmek amacıyla piezoelektrik eyleyiciler de kullanılmıştır. Anten kolu, alüminyumdan yapılmış dört yüzeyi piezoelektrik tabakayla kaplanmış dikdörtgen biçimindedir. Anten kolu, sonlu elemanlar kullanılarak modellenmiştir. Uydunun yönelim başarımı, çeşitli yönelim başarımı ölçütleri kullanılarak benzetimler aracılığıyla değerlendirilmiştir. Piezoelektrik eyleyicilerin etkinliği gösterilmiştir.

Anahtar Kelimeler: Aktif Kontrol Sistemi, Aktif Titreşim Kontrol Sistemi, Piezoelektrik, Piezoelektrik Malzemeler, Akıllı Esnek Kiriş Yapıları, Uzay Aracı Titreşimleri.

To My Family

ACKNOWLEDGEMENTS

First, I would like to express my deepest gratitude to my supervisor Prof. Dr. Ozan Tekinalp for giving me the opportunity to conduct this research and for his precious support and guidance. I gratefully thank also Asst. Prof. Dr. Ali Türker Kutay for his advises and support.

Very special thanks go to my family who has always supported me throughout my life. Their endless love, support and sacrifices have enabled this study's completion.

Finally, I would like to gratefully thank Zeynep Çakır and my colleagues in Space Systems and Technologies Department of Turkish Aerospace Industries Inc. (TAI) especially to Burak Akbulut and Emre Yurtoğlu for their unwavering support. Last but not least special thanks are for Teoman Güngör who is the manager of the Space Systems and Technologies Department and also for Dr. Erhan Solakoğlu, who encouraged me to start with the graduate education.

TABLE OF CONTENTS

ABSTRACT iv
ÖZ..... v
ACKNOWLEDGEMENTS vii
TABLE OF CONTENTS viii
LIST OF TABLES x
LIST OF FIGURES xi
LIST OF SYMBOLS xiii
1 INTRODUCTION 1
1.1. Motivation 2
1.2. Literature Survey 3
1.2.1. Active Vibration Control Systems 3
1.2.2. Smart Structures 4
1.2.3. Piezoelectricity 5
1.3. Contributions of the Thesis 7
1.4. Thesis Outline 8
2 MATHEMATICAL MODEL OF A SATELLITE WITH PIEZOELECTRIC SMART BEAM 9
2.1. Finite Element Model of a Flexible Beam with Fully Distributed Piezoelectric Layers 9
2.2. Formulation of Piezoelectric Smart Beam Element 11
2.3. Feedback Control Algorithm 20
2.3.1. Linear Quadratic Regulator (LQR) Control System 20
2.4. Pointing Performance 23
2.4.1. Performance Metrics Definitions 23
2.5. Algorithms of Metrics 25
3 RESULTS AND DISCUSSION 28

3.1. Simulation Code 28
3.2. Simulation Results 32
3.2.1. Case Study 1: Feedback Control without a Tip Mass - No PZT Actuators 32
3.2.2. Case Study 2: Feedback Control with a Tip Mass - No PZT Actuators 36
3.2.3. Case Study 3: Feedback Control without a Tip Mass (There is PZT Actuator Control) 40
3.2.4. Case Study 4: Feedback Control with a Tip Mass (There is PZT Actuator Control) 49
4 SUMMARY AND CONCLUSION 56
4.1. Summary 56
4.2. Conclusion 56
4.3. Suggestions for Future Work 57
REFERENCES 58

LIST OF TABLES

TABLES

Table 1.1: Examples of pointing accuracy for Earth observation satellites 1
Table 2.1: Properties of Beam and Piezoelectric Material 17
Table 2.2: Natural frequency comparison of the free-free beam with the analytic solutions in y and z axes 20
Table 3.1: Satellite accuracy, jitter and stability results (3σ) in 3 axes without a tip mass when there are no PZT actuators – 0.2 Nm torque input 34
Table 3.2: Satellite accuracy, jitter and stability results (3σ) in 3 axes without a tip mass when there are no PZT actuators – 0.1 Nm torque input 36
Table 3.3: Satellite accuracy, jitter and stability results (3σ) in 3 axes with a tip mass when there are no PZT actuators – 0.2 Nm torque input 38
Table 3.4: Satellite accuracy, jitter and stability results (3σ) in 3 axes with a tip mass when there are no PZT actuators – 0.1 Nm torque input 40
Table 3.5: Satellite accuracy, jitter and stability results (3σ) in 3 axes without a tip mass when low level disturbance torque input is applied 45
Table 3.6: Satellite accuracy, jitter and stability results (3σ) in 3 axes without a tip mass when high level disturbance torque input is applied 48
Table 3.7: Satellite accuracy, jitter and stability results (3σ) in 3 axes with a tip mass when low level disturbance torque input is applied 52
Table 3.8: Satellite accuracy, jitter and stability results (3σ) in 3 axes with a tip mass when high level disturbance torque input is applied 55

LIST OF FIGURES

FIGURES

Figure 1.1 TerraSAR-X long antenna boom demonstration 2
Figure 1.2: Examples of physical domains and associated energy conjugated state variables..... 4
Figure 2.1: Satellite-smart beam system 10
Figure 2.2: Satellite Dimensions 10
Figure 2.3: Illustration of the flexible beam piezoelectric layers discretized as four finite elements 11
Figure 2.4: Cross-section representation of the beam 11
Figure 2.5: Representation of pointing error for three imaging windows [28] 26
Figure 3.1: Simulink model of the satellite system 28
Figure 3.2: Satellite and flexible beam model..... 29
Figure 3.3: PZT actuator and state space models..... 30
Figure 3.4: PZT actuator model 30
Figure 3.5: Disturbance torque doublet applied to the satellite..... 31
Figure 3.6: The disturbance torque (first 1 s) and control torque in y direction applied to the satellite without tip mass - no PZT actuators 33
Figure 3.7: Satellite Euler attitude error without tip mass - no PZT actuators..... 33
Figure 3.8: Low level disturbance torque input 34
Figure 3.9: The disturbance torque (first 1 s) and control torque in y direction applied to the satellite without tip mass - no PZT actuators 35
Figure 3.10: Satellite Euler attitude error without tip mass - no PZT actuators.... 35
Figure 3.11: The disturbance torque (first 1 s) and control torque in y direction applied to the satellite with a tip mass - no PZT actuators..... 37
Figure 3.12: Satellite Euler attitude error with a tip mass - no PZT actuators..... 37
Figure 3.13: The disturbance torque (first 1 s) and control torque in y direction applied to the satellite with a tip mass - no PZT actuators..... 39
Figure 3.14: Satellite Euler attitude error with a tip mass - no PZT actuators..... 39

Figure 3.15: The disturbance torque (first 1 s) and control torque in y direction applied to the satellite without a tip mass 42
Figure 3.16: PZT actuator generated bending moments along y axis without a tip mass 42
Figure 3.17: Y-direction PZT actuator voltages - without a tip mass 43
Figure 3.18: Satellite Euler attitude error without a tip mass 43
Figure 3.19: Satellite angular velocity without a tip mass 44
Figure 3.20: Satellite angular acceleration without a tip mass 44
Figure 3.21: The disturbance torque (first 1 s) and control torque in y direction applied to the satellite without a tip mass 45
Figure 3.22: PZT actuator generated bending moments along y axis without a tip mass 46
Figure 3.23: Y-direction PZT actuator voltages - without a tip mass 46
Figure 3.24: Satellite Euler attitude error without a tip mass 47
Figure 3.25: Satellite angular velocity without a tip mass 47
Figure 3.26: Satellite angular acceleration without a tip mass 48
Figure 3.27: The disturbance torque (first 1 s) and control torque in y direction applied to the satellite with a tip mass 50
Figure 3.28: PZT actuator generated bending moments along y axis with a tip mass 50
Figure 3.29: Y-direction PZT actuator voltages - with a tip mass 51
Figure 3.30: Satellite Euler attitude error with a tip mass 51
Figure 3.31: The disturbance torque (first 1 s) and control torque in y direction applied to the satellite with a tip mass 53
Figure 3.32: PZT actuator generated bending moments along y axis with a tip mass 53
Figure 3.33: Y-direction PZT actuator voltages - with a tip mass 54
Figure 3.34: Satellite Euler attitude error with a tip mass 54

LIST OF SYMBOLS

m_s	Satellite mass (kg)
I_s	Satellite principal moment of inertia tensor (kg.m^2)
r_s	Length of the cubic satellite (m)
m_t	Mass of the tip mass (kg)
I_t	Moment of inertia tensor of tip mass (kg.m^2)
r_t	Radius of tip mass (m)
ρ_b	Mass density of the beam, Aluminum (kg/m^3)
E_b	Young's modulus of beam (N/m^2)
I_b	Moment of inertia of the beam cross-section
A_b	Beam cross-section area (m^2)
ρ_p	Mass density of the piezoelectric material (kg/m^3)
E_p	Young's modulus of piezoelectric element (N/m^2)
h_b	Height (thickness) of beam (m)
h_p	Height (thickness) of piezoelectric element (m)
w_b	Beam width (m)
w_p	Piezoelectric width (m)
I_p	Moment of inertia of the piezoelectric cross-section
A_p	Cross-section area of piezoelectric actuator (m^2)
L_b	Total beam length [m]
l_b	Length of each finite beam element (m)
d_{31}	Strain constant of piezoelectric material
g_{31}	Stress constant of piezoelectric material
$\vec{w}_{S/C}$	Satellite angular velocity vector (rad/s)
V_a	Applied Voltage (V)
Q	State weighting matrix
R	Input weighting matrix
$\vec{h}$	Angular momentum vector of satellite

CHAPTER 1

INTRODUCTION

Active control systems have many applications in various fields of engineering to achieve certain goals. One of the major applications is concerned with attenuation of unwanted vibrations and thus improving the pointing performance of the spacecraft observation instruments. Astronomical and Earth observation missions require precise pointing performances. The piezoelectric materials are one of the cost-effective solutions for reducing vibration levels [1] [2].

In a general fashion, some pointing accuracy examples of Earth observation satellites are represented in Table 1.1 [3] [4] [5] [6].

Table 1.1: Examples of pointing accuracy for Earth observation satellites

Satellite	**Pointing Accuracy (°)**	**Attitude Jitter (°/sec)**
Radarsat 1 (1995) [3]	±0.1°	-
TerraSAR-X (2007) [4]	0.018056° (3σ) 65 arcsec	-
GeoEye1 (2008) [5]	0.020833° (3σ) (75 arcsec)	0.000001944°/sec (0.007 arcsec/s rms (25 - 2000 Hz))
EO-1 (2000) [6]	0.03°	0.0013889 < 5 arcseconds

A satellite boom demonstration of TerraSAR-X satellite is depicted in Figure 1.1 [7].

Figure 1.1 TerraSAR-X long antenna boom demonstration

There are many vibration sources in a satellite such as reaction wheels, thrusters, solar array mechanism and other articulating devices of which vibration levels may exceed certain requirements [8]. In addition to internal disturbances, the external ones (solar radiation pressure, atmospheric drag, magnetic field etc.) also effect adversely the satellite pointing accuracy in a certain amount.

In this scope, this thesis study mainly focuses on the active vibration control of a satellite system with a flexible piezo-layered beam to attenuate the unwanted vibrations and to improve the satellite pointing performance.

1.1. Motivation

Sub-meter ground sampling distance for Earth observation space missions has been a subject of intensive work in recent years. Within this scope, high precision pointing performance of spacecraft instruments (satellite camera, telescopes, etc.) is necessary to achieve the desired spatial resolution.

For a satellite, the attitude control system is responsible for the desired pointing performance. For instance, reaction wheels and thrusters are the usual actuators on

satellite to point the satellite with certain accuracy. The thrusters on satellite consume fuel that limits the satellite functional life. Excessive actuator activity by reaction wheels may result in wearing them out much earlier [9].

In general, satellites may have light and very flexible structures which have small material damping. Such systems may cause poor pointing performance as well. In order to overcome such problems, the active vibration control of such flexible spacecraft parts may be considered.

The piezoelectric materials are well-known smart materials used in the field of active vibration control in recent years. Thus, a closed loop active vibration control system using the piezoelectric materials may be a meaningful approach to improve the pointing accuracy of a satellite.

This thesis addresses an active vibration control system that uses both attitude and structure control.

1.2. Literature Survey

1.2.1. Active Vibration Control Systems

There exist numerous studies regarding the active vibration control in flexible beam type structures.

Narayanan and Balamurugan [10] studied the finite element model of piezolaminated smart structures for the active vibration control of beams, plates and shells.

Vasques and Rodrigues [11] investigated and analyzed the active vibration control of smart three-layered piezoelectric beams by comparing the classical and optimal

feedback control strategies (constant gain, amplitude velocity feedback, LQR and LQG controllers).

L. Malgaca [12] presented numerical and experimental studies on the active vibration control of mechanical systems and piezoelectric smart structures. Closed loop control logics are incorporated into the finite element (FE) models by using ANSYS parametric design language (APDL).

1.2.2. Smart Structures

The extensive investigation for intelligent structures called as smart structures have been conducted by many researchers in recent years because of their useful applications in numerous structures. These smart structures take the advantages of smart materials such as Piezoelectrics, Magneto-Rheological Fluids, Piezo-ceramics, Electro-Rheological Fluids, Shape Memory Alloys, PVDF (Poly Vinylidene Fluoride), Optical fibers, etc. [13].

As pointed out in [14], smart materials are defined as the materials that convert energy between multiple physical domains such that piezoelectric materials convert mechanical energy to electric energy and vice versa.

Mechanical	Electrical	Thermal	Magnetic	Chemical
Stress	Electric field	Temperature	Magnetic field	Concentration
Strain	Electric displacement	Entropy	Magnetic flux	Volumetric flux

Figure 1.2: Examples of physical domains and associated energy conjugated state variables

In structural control applications, the piezoelectric materials are the most popular and widely used smart materials as distributed high precision actuators and sensors for a wide range of frequencies since the potential use of the best known piezoceramic PZT discovered in 1954 by Jaffe [14].

M. Moshrefi-Torbati, A.J. Keane, S.J. Elliott, M.J. Brennan, D.K. Anthony, E. Rogers [15] studied the structure of a 4.5 m long satellite boom consisting of 10 identical bays with equilateral triangular cross sections from the active vibration control point of view using experimental measurements incorporated with the computational predictions.

A. Zabihollah, R. Sedagahti and R. Ganesan [16] reported a study on vibration suppression of laminated composite beams using the smart structures piezoceramic and PVDF patches as the actuation and sensing elements. A finite element model based on the layerwise displacement theory associated with the state space model of the active laminated beam based on LQR was designed. Experimental studies conducted and compared with the corresponding simulation results.

1.2.3. Piezoelectricity

Piezoelectric effects are well known as Jaffe states that "the generation of electric charge in a substance by a mechanical stress that changes its shape and a proportional change in the shape of a substance when voltage is applied." These two effects discovered by brothers Curie around 1880 [17].

From material point of view, piezoelectric actuators are split into two. One is ceramic and the other one is polymer type. Both have the same principle [18]. Although piezoelectric polymers have comparatively low electromechanical coupling behavior mainly used for sensing purposes, piezoelectric ceramics may be used for both sensing and actuation, as in the case of self-sensing actuators [17]. For these reasons, piezoelectric ceramic discovered in the 1950's is taken into consideration for the active vibration control system developed within this study thanks to the many advantages over the other piezoelectric type materials as given in the following [14] [19] [20] [21];

- Unlimited Resolution (sub-nanometer precision)
- High bandwidths
- Large Force Generation
- Fast Response
- Good recoverable strain (up to 0.1%)
- No Magnetic Fields
- Low Power Consumption
- Vacuum and Clean-Room Compatible
- Operation at Cryogenic Temperatures

The most popular piezoelectric ceramic PZT (Lead Zirconate Titanate) shows a very strong piezo-effect. Piezoelectric material mentioned in the context of this thesis is referred to PZT.

In order to clarify the PZT concept and the ways through which active control algorithms are employed, the following expressions are introduced next.

Concerning the electromechanical properties of smart structures, there exist direct and the converse effects of piezoelectric material. In short, if an electric field is applied, a mechanical strain is generated which is known as the converse effect and conversely if a mechanical stress is subjected, an electric charge is produced as a result of mechanical response of the structure which is called direct effect as described in literature [13] [17].

The coefficients d and g are very significant properties of the piezoelectric material in terms of the performance criteria to be used as a smart material. When a voltage applied and electric field is available a high d and a high g are desired parameters for increasing performance of the actuators and the sensors [22].

Recent extensive applications of piezoelectric materials in smart structures of which main applications are the control of disturbing vibrations [17] are very important to elaborate on their mechanism as actuators and sensors. There are various analytical and experimental studies regarding the piezoelectric. Some of these scientific papers are presented next.

D. R. Fay [21] reported a scientific paper on vibration control of a smart cantilever beam based on piezoelectric concept. Linear Quadratic Gaussian (LQG) theory resulting in high-order controllers and optimal control theory were being employed to directly optimize low-order controllers.

Q. Hu and G. Ma [23] analyzed the vibration reduction of flexible spacecraft during attitude maneuver by using the variable structure control (VSC) theory to design switching logic for thruster firing and PZT as sensor and actuator for active vibration suppression.

In recent years, two common beam theories are studied within the concept of the smart structural mechanics which are the Euler Bernoulli and the Timoshenko beam models. In this study, the classical Euler Bernoulli beam theory is considered and the details are presented in Chapter 2.

1.3. Contributions of the Thesis

The contributions of thesis study are:

- A hypothetical satellite with a flexible boom with bonded PZT layers on all four surfaces is modeled

- A simulation code for the spacecraft-boom system is developed in Matlab/Simulink

- LQR type feedback control is designed

- Effectiveness of PZT actuator on pointing performance is demonstrated through simulations.

1.4. Thesis Outline

The organization of this thesis report is presented as follows:

In Chapter 1, a basic overview, the motivation of the study and the literature survey are presented briefly.

In Chapter 2, the mathematical model of a flexible beam with a number of PZT elements bonded on all four surfaces of the rectangular beam is developed using finite element method. The active vibration control system based on Linear Quadratic Regulator (LQR) technique is described. Also, the pointing performance of the system is presented through pointing metrics.

In Chapter 3, numerous simulation studies for different cases are carried out and the simulation results are discussed.

In Chapter 4, the main conclusions and future work plan are given.

CHAPTER 2

MATHEMATICAL MODEL OF A SATELLITE WITH PIEZOELECTRIC SMART BEAM

In this chapter, first a detailed mathematical model of the satellite together with the flexible smart beam and a tip mass is developed using finite element method. Then, the feedback control based on LQR control method is shortly presented. Finally, the satellite pointing metrics together with the formulations utilized in simulation code are given.

2.1. Finite Element Model of a Flexible Beam with Fully Distributed Piezoelectric Layers

Based on the Hamilton theory and the finite element discretization method, a rigid satellite and a flexible smart beam with a tip mass are studied in the context of this thesis. It is assumed that the beam is thin, the rotation and shear deformations are neglected which refers to the classical Euler-Bernoulli beam assumption. Only bending deformations due to the satellite maneuver are taken into account. No structural damping is included in the model.

The external disturbances (aerodynamic, magnetic field, solar pressure etc.) are not taken into account in the model since they are rather small.

The satellite-beam system is shown in Figure 2.1.

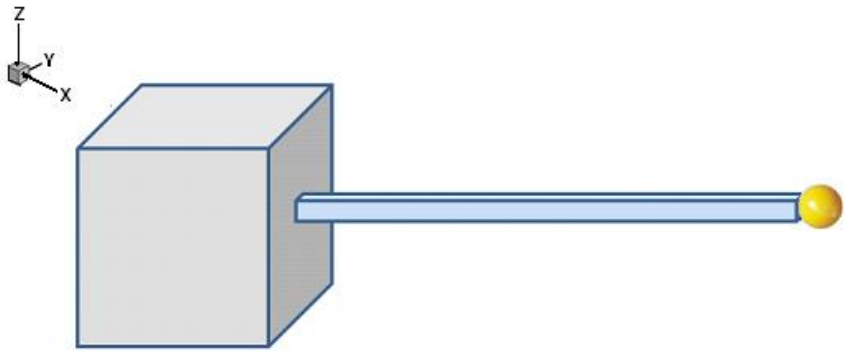

Figure 2.1: Satellite-smart beam system

The dimensions of the cubic satellite are given in Figure 2.2.

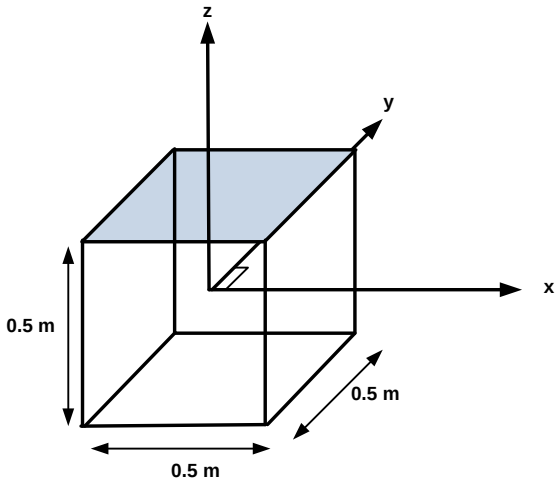

Figure 2.2: Satellite Dimensions

The satellite mass is 200 kg and the satellite moment of inertia tensor can be written as:

$$I_{S/C} = \begin{bmatrix} 8.3333 & 0 & 0 \\ 0 & 8.3333 & 0 \\ 0 & 0 & 8.3333 \end{bmatrix} \text{kg.m}^2 \qquad (2.1)$$

The finite element discretization model of the smart beam together with piezoelectric layers in both y and z axes is illustrated in Figure 2.3.

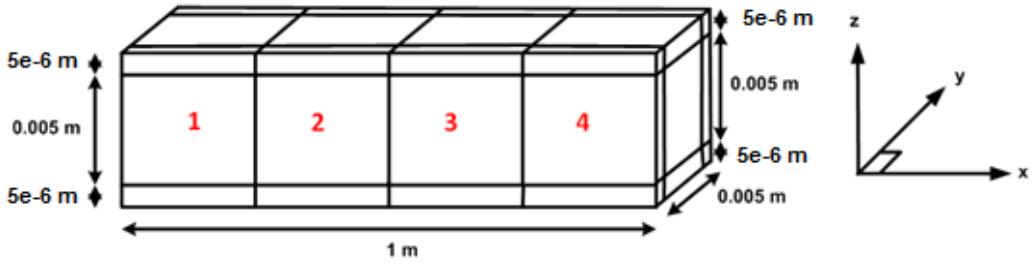

Figure 2.3: Illustration of the flexible beam piezoelectric layers discretized as four finite elements

The cross-section of the beam structure is demonstrated in Figure 2.4. Piezoelectric layers are bonded on all four surfaces of the Aluminum rectangular beam with the dimensions shown.

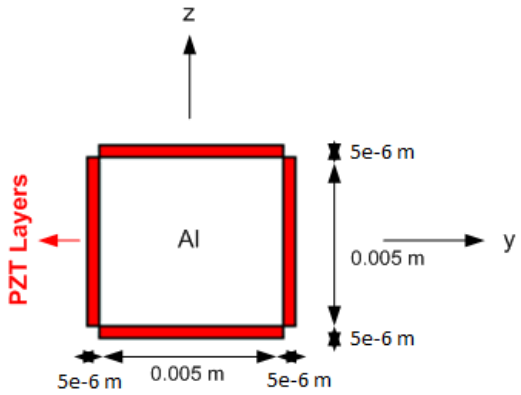

Figure 2.4: Cross-section representation of the beam

2.2. Formulation of Piezoelectric Smart Beam Element

A finite element formulation is carried out to model the dynamic behavior of the flexible beam structure with surface bonded piezoelectric layers subjected to both electrical and mechanical loadings. This formulation is based on the classical Euler-Bernoulli beam assumption.

With this finite element formulation, mass and stiffness matrices of all satellite system are obtained by taking into account the mass and stiffness contribution of the piezo-layers as well. 4 finite beam elements are considered. In this case, there

are 5 nodes for y and z directions separately; every node has two transverse deflections (in y and z directions). In this case, the axial and torsional deformations (in x direction) are not taken into consideration.

Based on the satellite model shown in Figure 2.1, total transverse velocity of a mass element on the flexible beam can be computed as follows [24];

$$v(x,t) = \dot{w}(x,t) + (x+r)\dot{\theta}\ (t) \tag{2.2}$$

where x represents the variable measured from the outer surface of the rigid satellite along the undeformed beam axis, $\theta(t)$ is the satellite rotation angle, $w(x,t)$ is the deflection measured from the x axis and overdots show the derivatives with respect to time t.

The beam structure is assumed to be rigidly and perfectly fixed and aligned with the satellite center of mass.

As stated before, making Euler-Bernoulli beam theory assumption and considering small deformation, the total kinetic and potential energy may be written as [24];

$$T = \frac{1}{2} I_{S/C} \dot{\theta}^2 + \frac{1}{2} \int_0^L \rho v^2\, dx + \frac{1}{2} m_{tip} v^2(L) + \frac{1}{2} I_{tip} \left(\frac{\partial v}{\partial x}\Big|_L\right)^2 \tag{2.3}$$

$$V = \frac{1}{2} \int_0^L EI \left(\frac{\partial^2 w}{\partial x^2}\right)^2 dx \tag{2.4}$$

Taking into account the satellite rotational torque and the PZT actuation moment u_1 and u_2 respectively, the virtual work is written as [24];

$$\delta W = u_1 \delta\theta(t) + u_2 [\delta\theta + \delta \left(\frac{\partial w}{\partial x}\Big|_L\right)] \tag{2.5}$$

According to the Hamilton's principle, the first variations of the equations above may be written as [24];

$$\int_{t_1}^{t_2}\Bigg[\int_0^L \rho\left(\dot{w}+(x+r_s)\dot{\theta}\right)\left(\delta\dot{w}+(x+r_s)\delta\dot{\theta}\right)dx-\int_0^L EI\left(\frac{\partial^2 w}{dx^2}\right)\delta\left(\frac{\partial^2 w}{dx^2}\right)dx+ m_{tip}\left(\dot{w}(L)+(L+r_s)\dot{\theta}\right)\left(\delta\dot{w}(L)+(L+r_s)\delta\dot{\theta}\right)+I_{tip}\left(\frac{\partial\dot{w}}{\partial x}\Big|_L+\dot{\theta}\right)\Big[\delta\frac{\partial\dot{w}}{\partial x}\Big|_L+ \delta\dot{\theta}\Big]+I_s\dot{\theta}\delta\dot{\theta}+u_1\delta\theta+u_2\left[\delta\theta+\delta(\frac{\partial w}{\partial x}\Big|_L)\right]\Bigg]dt=0 \tag{2.6}$$

After integrating the equation becomes;

$$\int_{t_1}^{t_2}\Big[\int_0^L\Big[\rho\left(\ddot{w}+(x+r_s)\ddot{\theta}\right)\delta w+EI\left(\frac{\partial^2 w}{dx^2}\right)\delta\left(\frac{\partial^2 w}{dx^2}\right)\Big]dx+\Big\{\int_0^L\rho\,(x+r_s)\left(\ddot{w}+(x+ r_s)\ddot{\theta}\right)dx+I_s\ddot{\theta}+m_{tip}(L+r_s)\left\{\ddot{w}(L)+(L+r_s)\ddot{\theta}\right\}+I_{tip}\left(\frac{\partial\ddot{w}}{\partial x}\Big|_L+\ddot{\theta}\right)- (u_1+u_2)\Big\}\delta\theta+\ m_{tip}\left\{\ddot{w}(L)+(L+r_s)\ddot{\theta}\right\}\delta w(L)+\Big[I_{tip}\left(\frac{\partial\ddot{w}}{\partial x}\Big|_L+\ddot{\theta}\right)- u_2\Big]\delta\frac{\partial w}{\partial x}\Big|_L\Big]dt=0 \tag{2.7}$$

The generalized state space representation of the system composed of a satellite, a piezoelectric smart beam with a tip mass modeled is given below [24];

$$\begin{bmatrix}I_s+M_{\theta\theta} & M_{\theta v}\\ M_{v\theta} & M_{vv}\end{bmatrix}\begin{Bmatrix}\ddot{\theta}\\ \ddot{v}\end{Bmatrix}+\begin{bmatrix}0 & 0\\ 0 & K_{vv}\end{bmatrix}\begin{Bmatrix}\theta\\ v\end{Bmatrix}=\begin{bmatrix}1 & 1\\ 0 & 0\end{bmatrix}\begin{Bmatrix}u_1\\ u_2\end{Bmatrix} \tag{2.8}$$

where v denotes both the transverse deflection and rotation angle of the beam. In this formula, the notations show the following mass and stiffness matrices for four finite elements ($N=4$):

$$M_{\theta\theta}=\sum_{i=1}^{N}M_{11}^{i}+M_{11}^{t}=M_{11}^{1}+M_{11}^{2}+M_{11}^{3}+M_{11}^{4}+M_{11}^{t} \tag{2.9}$$

where superscript "i" indicates the element number and "t" indicates the tip mass

$$M_{\theta v} = \begin{bmatrix} M_{13}^1 + M_{12}^2 & M_{13}^2 + M_{12}^3 & M_{13}^3 + M_{12}^4 & M_{13}^4 + M_{12}^t \end{bmatrix} \quad (2.10)$$

$$M_{vv} = \begin{bmatrix} M_{33}^1 + M_{22}^2 & M_{23}^2 & 0 & 0 \\ M_{32}^2 & M_{33}^2 + M_{22}^3 & M_{23}^3 & 0 \\ 0 & M_{32}^3 & M_{33}^3 + M_{22}^4 & M_{23}^4 \\ 0 & 0 & M_{32}^4 & M_{33}^4 + M_{22}^t \end{bmatrix} \quad (2.11)$$

$$K_{vv} = \begin{bmatrix} K_{33}^1 + K_{22}^2 & K_{23}^2 & 0 & 0 \\ K_{32}^2 & K_{33}^2 + K_{22}^3 & K_{23}^3 & 0 \\ 0 & K_{32}^3 & K_{33}^3 + K_{22}^4 & K_{23}^4 \\ 0 & 0 & K_{32}^4 & K_{33}^4 \end{bmatrix} \quad (2.12)$$

Local mass and stiffness matrices of a flexible beam element are given in the following equations [24]:

$$M_e^i = \begin{bmatrix} M_{11}^i & M_{12}^i & M_{13}^i \\ M_{21}^i & M_{22}^i & M_{23}^i \\ M_{31}^i & M_{32}^i & M_{33}^i \end{bmatrix} \quad (2.13)$$

$$K_e^i = \begin{bmatrix} 0 & 0 & 0 \\ 0 & K_{22}^i & K_{23}^i \\ 0 & K_{32}^i & K_{33}^i \end{bmatrix} \quad (2.14)$$

where

$$M_{11}^i = \frac{\rho A l}{3}\{(x_i + r_s)^2 + (x_i + r_s + l)(x_i + r_s) + (x_i + r_s + l)^2\} \quad (2.15)$$

$$M_{12}^i = \left[M_{21}^i\right]^T = \rho A l \left[\frac{3}{20}l + \frac{1}{2}(x_i + r_s) \quad \frac{1}{30}l^2 + \frac{1}{12}l(x_i + r_s)\right] \quad (2.16)$$

$$M_{13}^i = \left[M_{31}^i\right]^T = \rho A l \left[\frac{7}{20}l + \frac{1}{2}(x_i + r_s) \quad -\frac{1}{20}l^2 - \frac{1}{12}l(x_i + r_s)\right] \quad (2.17)$$

$$M_{22}^i = \frac{\rho A l}{420}\begin{bmatrix} 156 & 22l \\ 22l & 4l^2 \end{bmatrix} \quad (2.18)$$

$$M_{23}^{i} = \left[M_{32}^{i}\right]^{T} = \frac{\rho A l}{420}\begin{bmatrix} 54 & -13l \\ 13l & -3l^{2} \end{bmatrix} \tag{2.19}$$

$$M_{33}^{i} = \frac{\rho A l}{420}\begin{bmatrix} 156 & -22l \\ -22l & 4l^{2} \end{bmatrix} \tag{2.20}$$

$$K_{22}^{i} = \frac{EI}{l^{3}}\begin{bmatrix} 12 & 6l \\ 6l & 4l^{2} \end{bmatrix} \tag{2.21}$$

$$K_{23}^{i} = \left[K_{32}^{i}\right]^{T} = \frac{EI}{l^{3}}\begin{bmatrix} -12 & 6l \\ -6l & 2l^{2} \end{bmatrix} \tag{2.22}$$

$$K_{33}^{i} = \frac{EI}{l^{3}}\begin{bmatrix} 12 & -6l \\ -6l & 4l^{2} \end{bmatrix} \tag{2.23}$$

Mass matrix of the tip mass is obtained as follows [24];

$$M_{t} = \begin{bmatrix} M_{11}^{t} & M_{12}^{t} \\ M_{21}^{t} & M_{22}^{t} \end{bmatrix} \tag{2.24}$$

where;

$$M_{11}^{t} = I_{t} + m_{t}\,(r_{s} + L)^{2} \tag{2.25}$$

$$M_{12}^{t} = \left[M_{21}^{t}\right]^{T} = \begin{bmatrix} m_{t}\,(r_{s} + L) & I_{t} \end{bmatrix} \tag{2.26}$$

$$M_{22}^{t} = \begin{bmatrix} m_{t} & 0 \\ 0 & I_{t} \end{bmatrix} \tag{2.27}$$

In above formulas, L represents the total beam length, r_s is the distance from the satellite center of mass to the beam root, A indicates the cross-section area, l is the length of the finite element, x_i is the distance from the root of the beam to the left end of the ith finite element similar to the definitions given in reference [24]. Due to change of x_i distance for each element of the beam, mass element matrices are different from each other. Since the entire beam is divided into 4 finite elements together with the piezoelectric elements bonded on each beam element separately, each has the same width and length with each beam element except for the

thickness (or height). At this point, the corresponding x_i distances for each element are taken as respectively:

$$x_1 = 0\ x_2 = l\ x_3 = 2l\ x_4 = 3l$$

Furthermore, each beam element has the same length which corresponds to $l = \frac{L}{4}$.

The flexural rigidity (EI) and mass per unit length (ρA) effects of the PZT layers are included in the model as given in the following equations [13];

$$EI = E_b I_b + 2E_p I_p \tag{2.28}$$

$$\rho A = \rho_b A_b + 2\rho_p A_p \tag{2.29}$$

The piezoelectric control force and the bending control moment equations of the piezoelectric actuators may be written as [10];

$$F_a = E_a d_{31} w V_a \tag{2.30}$$

$$M_a = r_a E_a d_{31} w V_a \tag{2.31}$$

where $r_a = \frac{h_a + h_b}{2}$ (h_a and h_b indicate the height of the PZT actuator and the beam respectively), E_a is the Young's Modulus of PZT actuator, d_{31} is the strain constant of PZT material, w is the width of the PZT actuator, V_a is the applied voltage by PZT actuator.

When the voltages applied to the PZT actuators, upper part of the beam structure is expanded while the lower part is contracted which results in the deformation of the beam structure.

The properties of the beam structure and the PZT material used in the simulation model are given in Table 2.1 [10].

Table 2.1: Properties of Beam and Piezoelectric Material

Beam Properties		**Piezoelectric Material Properties**	
E_b (Young's Modulus of Beam)	758×10^8 N/m^2	E_{pzt} (Young's Modulus of Piezoelectric Material)	139×10^9 N/m^2
ρ_b (Density of Beam)	2743 kg/m^3	ρ_{pzt} (Density)	7500 kg/m^3
L (Beam Length)	1 m	L_{pzt} (Length of Piezoelectric Material)	1 m
h (Beam Height)	5×10^{-3} m	h_{pzt} (Height of PZT Material)	5×10^{-6} m
w (Beam Width)	5×10^{-3} m	w_{pzt} (Width of PZT Material)	5×10^{-3} m
		d_{31} (Strain Constant of PZT Material)	11×10^{-11} m/V
		g_{31} (Stress Constant of PZT Material)	0.01 Vm/N

Using Equation (2.8), the mass and stiffness matrices of the satellite system with a tip mass (tip mass is 90 gram and radius is 20 mm) at the free end of the beam are derived as follows;

$$M_y$$

$$= \begin{bmatrix} 8.5185 & 0.0086 & 7.1823e-5 & 0.0129 & 7.1823e-5 & 0.0172 & 7.1823e-5 & 0.1226 & -3.9858e-4 \\ 0.0086 & 0.0128 & 0 & 0.0022 & -1.3339e-4 & 0 & 0 & 0 & 0 \\ 7.1823e-5 & 0 & 2.0521e-5 & 1.3339e-4 & -7.6953e-6 & 0 & 0 & 0 & 0 \\ 0.0129 & 0.0022 & 1.3339e-4 & 0.0128 & 0 & 0.0022 & -1.3339e-4 & 0 & 0 \\ 7.1823e-5 & -1.3339e-4 & -7.6953e-6 & 0 & 2.0521e-5 & 1.3339e-4 & -7.6953e-6 & 0 & 0 \\ 0.0172 & 0 & 0 & 0.0022 & 1.3339e-4 & 0.0128 & 0 & 0.0022 & -1.3339e-4 \\ 7.1823e-5 & 0 & 0 & -1.3339e-4 & -7.6953e-6 & 0 & 2.0521e-5 & 1.3339e-4 & -7.6953e-6 \\ 0.1226 & 0 & 0 & 0 & 0 & 0.0022 & 1.3339e-4 & 0.0964 & -2.2573e-4 \\ -3.9858e-4 & 0 & 0 & 0 & 0 & -1.3339e-4 & -7.6953e-6 & -2.2573e-4 & 2.4660e-5 \end{bmatrix}$$

$$K_y = \begin{bmatrix} 0 & 0 & 0 & 0 & 0 & 0 & 0 & 0 & 0 \\ 0 & 6.064e+3 & 0 & -3.0320e+3 & 379 & 0 & 0 & 0 & 0 \\ 0 & 0 & 126.3333 & -379 & 31.5833 & 0 & 0 & 0 & 0 \\ 0 & -3.0320e+3 & -379 & 6.064e+3 & 0 & -3.0320e+3 & 379 & 0 & 0 \\ 0 & 379 & 31.5833 & 0 & 126.3333 & -379 & 31.5833 & 0 & 0 \\ 0 & 0 & 0 & -3.0320e+3 & -379 & 6.0640e+3 & 0 & -3.0320e+3 & 379 \\ 0 & 0 & 0 & 379 & 31.5833 & 0 & 126.3333 & -379 & 31.5833 \\ 0 & 0 & 0 & 0 & 0 & -3.0320e+3 & -379 & 3.0320e+3 & -379 \\ 0 & 0 & 0 & 0 & 0 & 379 & 31.5833 & -379 & 63.1667 \end{bmatrix}$$

$$M_z$$

$$= \begin{bmatrix} 8.5185 & 0.0086 & 7.1823e-5 & 0.0129 & 7.1823e-5 & 0.0172 & 7.1823e-5 & 0.1226 & -3.9858e-4 \\ 0.0086 & 0.0128 & 0 & 0.0022 & -1.3339e-4 & 0 & 0 & 0 & 0 \\ 7.1823e-5 & 0 & 2.0521e-5 & 1.3339e-4 & -7.6953e-6 & 0 & 0 & 0 & 0 \\ 0.0129 & 0.0022 & 1.3339e-4 & 0.0128 & 0 & 0.0022 & -1.3339e-4 & 0 & 0 \\ 7.1823e-5 & -1.3339e-4 & -7.6953e-6 & 0 & 2.0521e-5 & 1.3339e-4 & -7.6953e-6 & 0 & 0 \\ 0.0172 & 0 & 0 & 0.0022 & 1.3339e-4 & 0.0128 & 0 & 0.0022 & -1.3339e-4 \\ 7.1823e-5 & 0 & 0 & -1.3339e-4 & -7.6953e-6 & 0 & 2.0521e-5 & 1.3339e-4 & -7.6953e-6 \\ 0.1226 & 0 & 0 & 0 & 0 & 0.0022 & 1.3339e-4 & 0.0964 & -2.2573e-4 \\ -3.9858e-4 & 0 & 0 & 0 & 0 & -1.3339e-4 & -7.6953e-6 & -2.2573e-4 & 2.4660e-5 \end{bmatrix}$$

$$K_z = \begin{bmatrix} 0 & 0 & 0 & 0 & 0 & 0 & 0 & 0 & 0 \\ 0 & 6.064e+3 & 0 & -3.0320e+3 & 379 & 0 & 0 & 0 & 0 \\ 0 & 0 & 126.3333 & -379 & 31.5833 & 0 & 0 & 0 & 0 \\ 0 & -3.0320e+3 & -379 & 6.064e+3 & 0 & -3.0320e+3 & 379 & 0 & 0 \\ 0 & 379 & 31.5833 & 0 & 126.7967 & -379 & 31.5833 & 0 & 0 \\ 0 & 0 & 0 & -3.0320e+3 & -379 & 6.064e+3 & 0 & -3.0320e+3 & 379 \\ 0 & 0 & 0 & 379 & 31.5833 & 0 & 126.3333 & -379 & 31.5833 \\ 0 & 0 & 0 & 0 & 0 & -3.0320e+3 & -379 & 3.0320e+3 & -379 \\ 0 & 0 & 0 & 0 & 0 & 379 & 31.5833 & -379 & 63.1667 \end{bmatrix}$$

According to the mass and stiffness matrices computed for both y and z axes of the beam structure; the natural frequencies of the finite element model are compared to the analytic results given in Table 2.2.

Table 2.2: Natural frequency comparison of the free-free beam with the analytic solutions in y and z axes

Analytic Solution (y axis)	**Finite Element Model (*N=4) (y axis)**	**Analytic Solution (z axis)**	**Finite Element Model (*N=4) (z axis)**
169.2931	166.9	169.2931	166.9
466.6465	470.5	466.6465	470.5
915.5925	928.1	915.5925	928.1

*: Number of elements

2.3. Feedback Control Algorithm

This subsection gives a general introductory overview for feedback control algorithm based on LQR method.

2.3.1. Linear Quadratic Regulator (LQR) Control System

The main objective of Linear Quadratic Regulator (LQR) is minimizing the cost function so that the control errors and the control effort can be reduced.

The LQR controller is designed based on the state-space representation. The states mentioned here are derived from the finite element modeling of the smart beam divided into 4 elements that results in 18 states for y and z axes in total.

The regulator is introduced as designing a control input (feedback form) to stabilize the plant about the zero state equilibrium point [24]. The linear regulator

problem is the most obvious special case of a linear system with the feedback control law being parameterized as a linear function of the instantaneous state. A linear first-order state space differential equation form is stated as [24];

$$\dot{x}(t) = Ax(t) + Bu(t) \tag{2.32}$$

where $x(t)$ is state vector, $u(t)$ is control vector mentioned in the preceding subsection, A is the system matrix (Equation (2.33)) and B is the control influence matrix. For the satellite model designed, the corresponding state-space matrices A and B are not time dependent, they are constant matrices with the size of [36x36] and [36x10] respectively.

$$[A] = \begin{bmatrix} 0 & I \\ -M^{-1}K & 0 \end{bmatrix} \tag{2.33}$$

where M and Krepresent the mass and stiffness matrices respectively.

For Linear Quadratic Regulator [25];

- The original system, $(A;B)$ must be controllable,
- The pair $(A;H)$ must be observable or all the states should be readily available , where $HH^T = Q$,
- The weighting matrices Q and R should be both symmetric, semi-positive definite and positive definite respectively.

The cost function can be written as;

$$J = \frac{1}{2}\int_0^\infty (x^T Q x + u^T R u) dt \tag{2.34}$$

The LQR gain matrix K of the state feedback control logic can be calculated by minimizing the cost function given in the equation (2.34) [26]:

$$u = -[K]\{x\} \tag{2.35}$$

Considering full state feedback, the control law can be expanded by the following equation:

$$u = -[K]\{x\} = -[R]^{-1}[B]^{T}[P]\{x\} \tag{2.36}$$

where $[K]$ is the control gain and $[P]$ is obtained from the following Algebraic Riccati equation;

$$[A]^{T}[P] + [P][A] - [P][B][R]^{-1}[B]^{T}[P] + [C_o]^{T}[Q][C_o] = 0 \tag{2.37}$$

The control input matrix of the satellite-boom system is as follows;

$$u = \begin{bmatrix} M_{S/C\_y} \\ M_{S/C\_z} \\ M_{b1\_y} \\ M_{b2\_y} \\ M_{b3\_y} \\ M_{b4\_y} \\ M_{b1\_z} \\ M_{b2\_z} \\ M_{b3\_z} \\ M_{b4\_z} \end{bmatrix} \tag{2.38}$$

where M_{S/C_y} and M_{S/C_z} indicate the satellite control torques in y and z axes and M_{b1_y} M_{b2_y}, M_{b3_y}, M_{b4_y}, M_{b1_z}, M_{b2_z}, M_{b3_z}, M_{b4_z} indicate the PZT actuator bending control moments for each beam element in y and z axes of the beam structure respectively.

In order to choose Q and R weighting matrices for the design of LQR control system, Bryson's Rule is considered such that [27];

$$Q = \begin{bmatrix} \frac{1}{\max \text{acceptable} value\ of\ (x_1^2)} & \cdots & 0 \\ \vdots & \ddots & \vdots \\ 0 & \cdots & \frac{1}{\max \text{acceptable} value\ of\ (x_N^2)} \end{bmatrix} \quad (2.39)$$

$$R = \begin{bmatrix} \frac{1}{\max \text{acceptable} value\ of\ (u_1^2)} & \cdots & 0 \\ \vdots & \ddots & \vdots \\ 0 & \cdots & \frac{1}{\max \text{acceptable} value\ of\ (u_N^2)} \end{bmatrix} \quad (2.40)$$

where x_i^2 indicates the states and u_i^2 indicates the inputs for $i = 1, \dots N$ (N is the total number of states)

2.4. Pointing Performance

Pointing, jitter and stability are very significant design parameters for the satellite imaging.

There exist several error sources affecting the satellite pointing performance. One of the major error sources is the slew-induced structural vibration due to the satellite maneuvers. The other error sources (reaction or momentum wheels, control moment gyroscopes, solar drive motors, thruster firing, cryogenic coolers etc.) are not of interest in this study.

2.4.1. Performance Metrics Definitions

In order to assess the pointing performance of the satellite model developed, the pointing performance metrics which are accuracy, stability and jitter metrics are described briefly.

As stated in the references [28] [29], there are several pointing metrics introduced in order to evaluate the satellite pointing performance. These metrics are accuracy, displacement, jitter, stability and windowed stability [28]. In this study, accuracy, jitter and stability metrics are considered.

According to Pittelkau [28], pointing error is the angular rotation from the desired pointing direction to the actual pointing direction in a short explanation the difference between both pointing directions.

After defining the pointing error, the descriptions of the fundamental pointing metrics are given as follows [28]:

- Accuracy (°) is the root mean square (RMS) of the pointing error. For the satellites, considering Euler rotational angles, the accuracy metric is calculated according to three body axes. The relevant formula is given;

$$\sqrt{{\sigma_a}^2 + \mu^2} \tag{2.41}$$

  where σ_a represents the variance and μ denotes the mean of pointing error.

- Jitter (°/s) is the root mean square pointing error within the jitter time window T_j. Jitter is an important parameter for imaging purposes in the sense of limiting blur, signal variation in a sensor, or for limiting some other measurement error. Jitter is denoted by σ_j.

- Stability (°) which is denoted by σ_s is the root mean square change in attitude from the beginning to the end of time interval T_s.

It is possible to calculate jitter metrics in either time or frequency domain. In this study, pointing performance computations were carried out in the frequency domain. The corresponding frequency domain formulas are defined in the next subsection.

As stated in [28], Euler attitude data obtained from the algorithms executed in simulation model is transformed to frequency domain via FFT (Fast Fourier Transform) algorithm in Matlab.

2.5. Algorithms of Metrics

In this subsection, the details of the metrics algorithms are investigated and the frequency domain formulas used in computations are presented in the upcoming expressions.

As reported in [28], for satellite imaging, there exist time dependencies of the image process. As illustrated in Figure 2.5, the satellite payloads generally are commanded to take image during the exposure time. Similarly, for the next imaging task, the previous image is registered in the satellite's memory during the readout time.

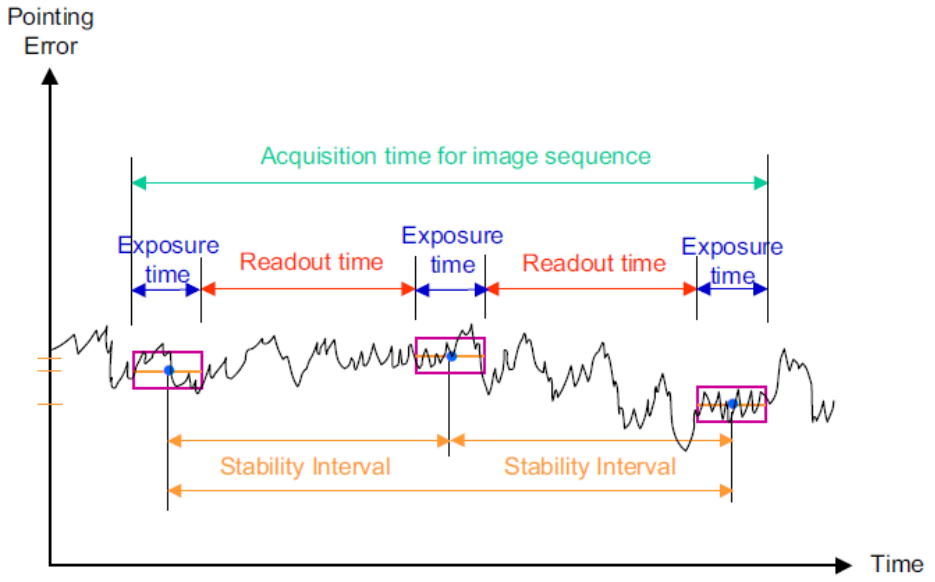

Figure 2.5: Representation of pointing error for three imaging windows [28]

Depending on these facts, for jitter calculation, the jitter time is assumed to be equal to exposure time (T_E). In addition, the stability time is taken as the sum of the exposure time and the readout time (T_{RO}) as designated in the following equations:

$$T_j = T_E \tag{2.42}$$

$$T_s = T_E + T_{RO} \tag{2.43}$$

The mathematical descriptions are given for accuracy, jitter and stability metrics respectively in the following formulas:

Attitude error metric algorithm is;

$$\sigma_a^2 + \mu^2 = \sum_{i=1}^{M} P(w_i) \tag{2.44}$$

Jitter metric formulation is;

$$\sigma_d^2(T_d) + \mu^2 = \sum_{i=1}^{M} P(w_i) W_j(w_i T_j) \tag{2.45}$$

Stability metric is formulated as;

$$\sigma_s^2(T_s) + \mu^2 = \sum_{i=1}^{M} P(w_i) W_s(w_i T_s) \quad (2.46)$$

where M is the length of data record,

$w = 2\pi[-M/2 : 1 : M/2 - 1]/M\delta$ represents the frequency range (rad/sec), δ is sample time (sec),

$P(w) = |FFTSHIFT(FFT(\theta, m))/M|^2$ denotes the power spectrum of θ,

$W_j(v) = 1 - 2(1 - cosv)/v^2$ is the jitter weighting function, $v = wT_j$,

$W_s(v) = 2(1 - cosv)$ is the stability weighting function, $v = wT_s$.

CHAPTER 3

RESULTS AND DISCUSSION

In this chapter, the simulation models developed in Matlab/Simulink are briefly described. Using different case studies, simulations are carried out and the results are discussed.

3.1. Simulation Code

The mathematical formulations of the satellite system are adapted into Matlab/Simulink model as demonstrated in Figure 3.1.

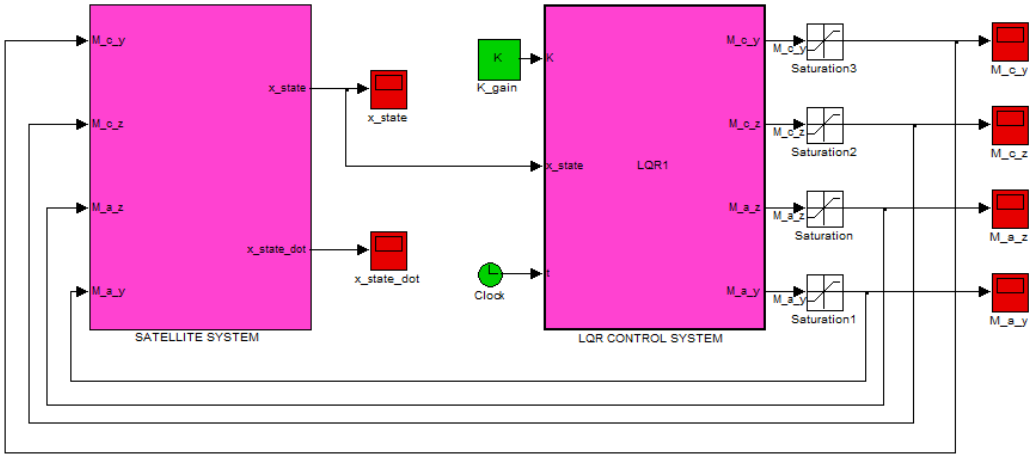

Figure 3.1: Simulink model of the satellite system

As seen from Figure 3.1, the simulink model basically consists of a satellite system and a LQR control algorithm blocks. Two saturation blocks for satellite control torques are added to the simulation model. ±0.3 Nm torque limit is considered for both M_c_y and M_c_z.

In the satellite system block depicted in Figure 3.2, the satellite with a flexible smart beam is modeled where *x_state* indicates the system states and similarly *x_state_dot* represents the derivative of the system states. The inputs of this model are the bending control moments of PZT actuators (M_a_z and M_a_y) and also the satellite control torques (M_c_y and M_c_z) due to slew maneuver in the corresponding axes.

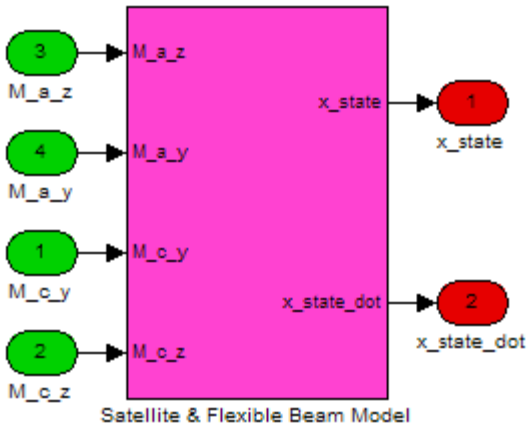

Figure 3.2: Satellite and flexible beam model

The satellite and the flexible beam model shown in Figure 3.3 are composed of the PZT actuators and the state space model blocks. System matrices A and B are computed in an M-file code and used as inputs for the state space representation. Hence, the system states together with their derivatives are obtained.

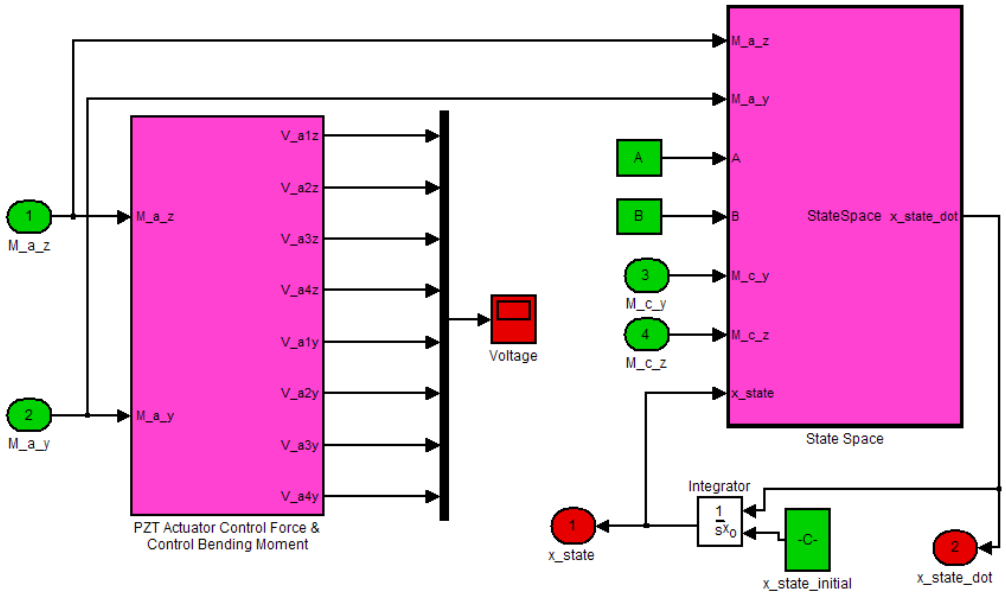

Figure 3.3: PZT actuator and state space models

Using equation (2.31), the applied voltages of the PZT actuators are calculated in the PZT actuator model as demonstrated in Figure 3.4.

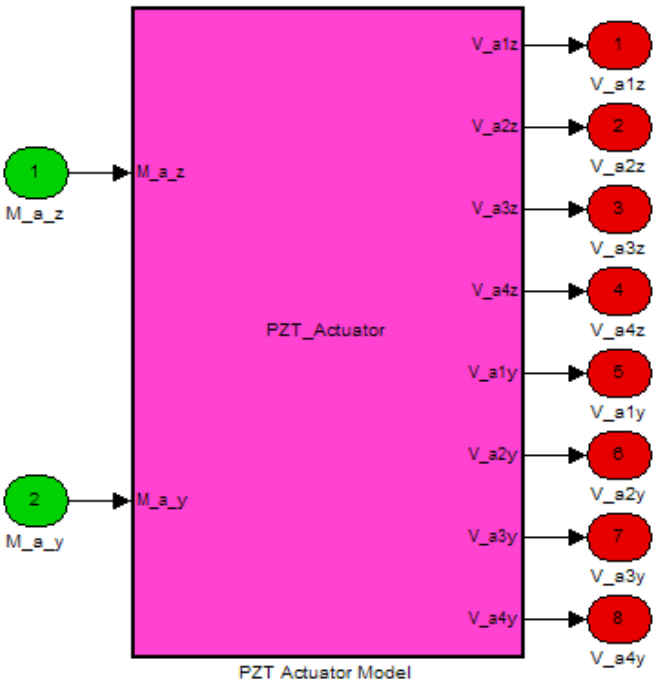

Figure 3.4: PZT actuator model

In addition, in the LQR control system model already shown in Figure 3.1, the control torques of the satellite and the bending control moments of the PZT actuators in both y and z axes are computed. The controller gain K is calculated in the M-file code generated using system (A, B) and the weighting matrices (Q, R) utilizing the command of $[K, P, e] = l\,qr\,(A, B, Q, R)$ where P indicates the matrix given in *Algebraic Riccati Equation* (2.37) and e indicates the closed loop eigenvalues.

"Variable step (Ode15 solver)" was used since the system is stiff. All simulations were performed for 30 seconds.

To evaluate controllers the disturbance torque input shown in Figure 3.5 is applied.

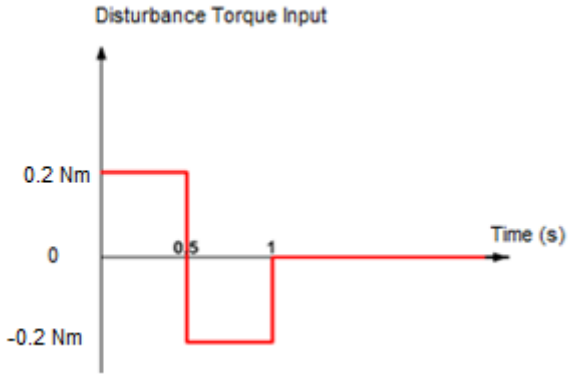

Figure 3.5: Disturbance torque doublet applied to the satellite

As can be seen from Figure 3.5, the disturbance torque doublet type input is given to the system with the constant amplitude of 0.2 Nm during the first 0.5 second. Then -0.2 Nm satellite torque is applied between 0.5 and 1 second. The disturbance torque level is set to zero afterwards. At 1.5 second the feedback control is initialized.

3.2. Simulation Results

For the simulation study, two M_file codes and a simulink model are developed. One of the M-File is to calculate the controller gain and the system matrices and the other one is to compute the satellite jitter performance results. Moreover, the results of the simulink model (Satellite Euler attitude error results) are supplied to another M-File code generated to obtain the satellite jitter, accuracy and the stability performance metrics.

In the following, simulation studies for different cases carried out are presented and discussed. Since there is coupling between y and z axes, the simulation results only in y axis are given.

3.2.1. Case Study 1: Feedback Control without a Tip Mass - No PZT Actuators

In this study, the feedback control based on the LQR controller is simulated without using a tip mass at the free end of the beam. In this case, only the satellite control torques in y and z axes are generated and no PZT actuator control is available. 0.2 Nm disturbance torque doublet input is applied as shown in Figure 3.5. The corresponding results are presented as follows.

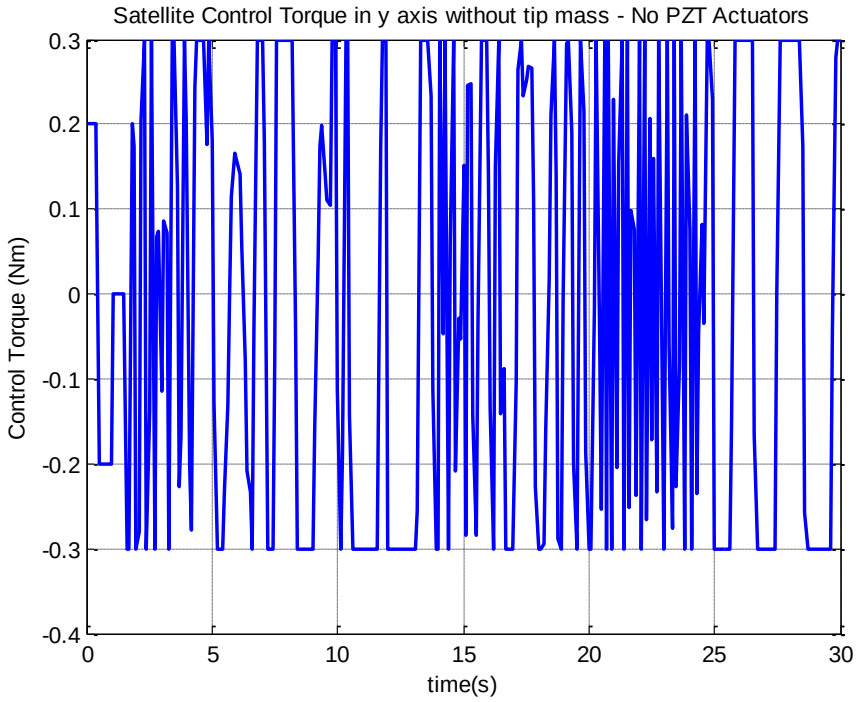

Figure 3.6: The disturbance torque (first 1 s) and control torque in y direction applied to the satellite without tip mass - no PZT actuators

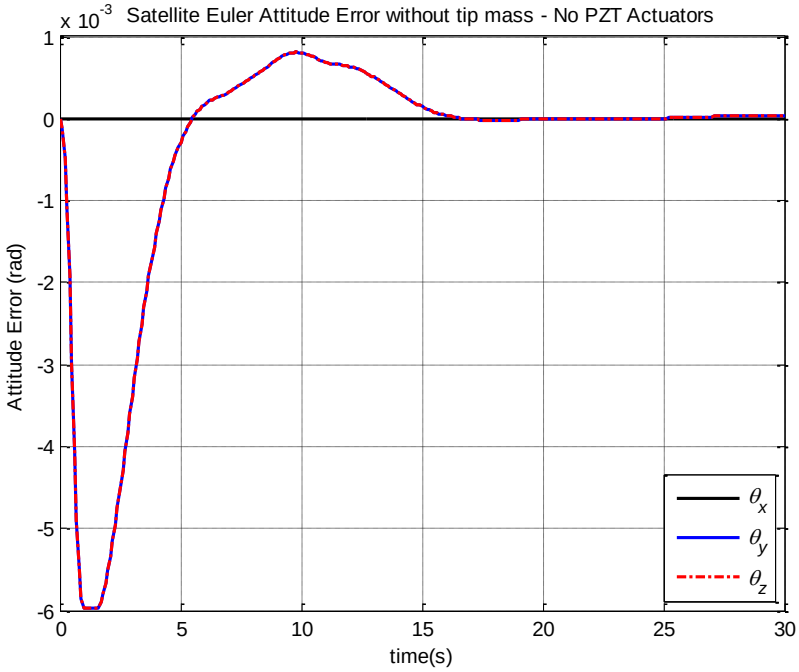

Figure 3.7: Satellite Euler attitude error without tip mass - no PZT actuators

As can be seen from Figure 3.6, the satellite control torque levels reach the saturation limits (±0.3 Nm) in lack of the PZT actuator control. According to the satellite Euler attitude error results given in Figure 3.7, the satellite pointing performance values are obtained as given in Table 3.1. These results are quite acceptable. However, actuator activity is quite high to wear out reaction wheels or deplete the fuel on board very rapidly.

Table 3.1: Satellite accuracy, jitter and stability results (3σ) in 3 axes without a tip mass when there are no PZT actuators – 0.2 Nm torque input

	Accuracy Metric (°)	**Jitter Metric (°/s) *10^{-3}**	**Stability Metric (°)**
x	0	0	0
y	0.0030	0.1875	0.0036
z	0.0030	0.1875	0.0036

When 0.1 Nm satellite disturbance torque input (Figure 3.8) is applied to the system, the system responses are given in the following.

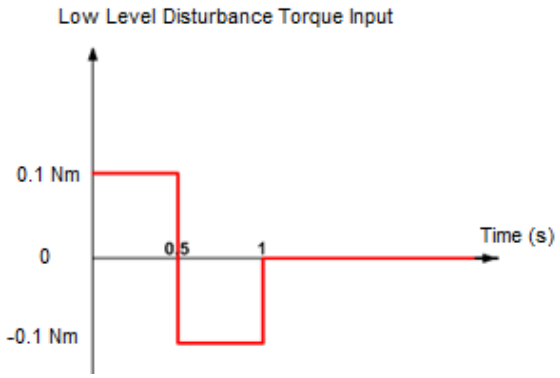

Figure 3.8: Low level disturbance torque input

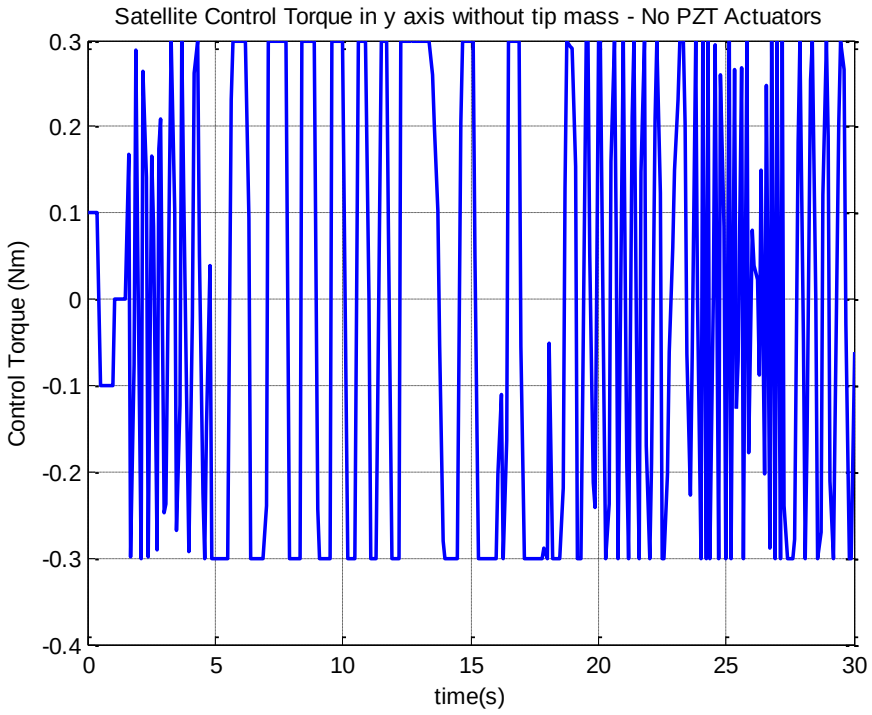

Figure 3.9: The disturbance torque (first 1 s) and control torque in y direction applied to the satellite without tip mass - no PZT actuators

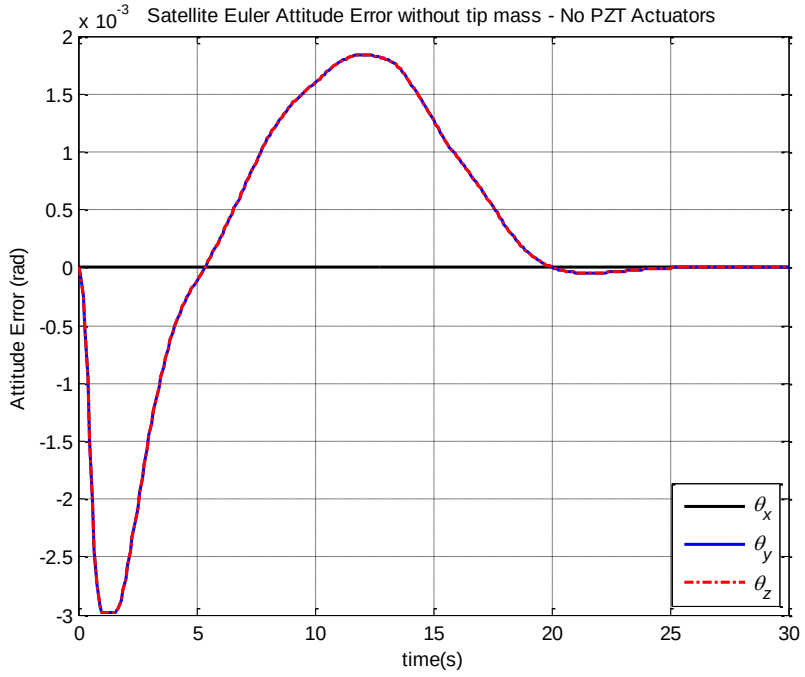

Figure 3.10: Satellite Euler attitude error without tip mass - no PZT actuators

Table 3.2: Satellite accuracy, jitter and stability results (3σ) in 3 axes without a tip mass when there are no PZT actuators – 0.1 Nm torque input

	Accuracy Metric (°)	**Jitter Metric (°/s) *10^{-3}**	**Stability Metric (°)**
x	0	0	0
y	0.0039	0.1038	0.0050
z	0.0039	0.1038	0.0050

Similar to the previous results obtained for 0.2 Nm torque input, the required control torques levels are at saturation limits and the actuator activity is too high as before.

3.2.2. Case Study 2: Feedback Control with a Tip Mass - No PZT Actuators

In this study, the feedback control in the lack of PZT actuators with a tip mass is analyzed through simulations. A high level satellite disturbance doublet is applied with the amount of 0.2 Nm. The corresponding results are given as follows.

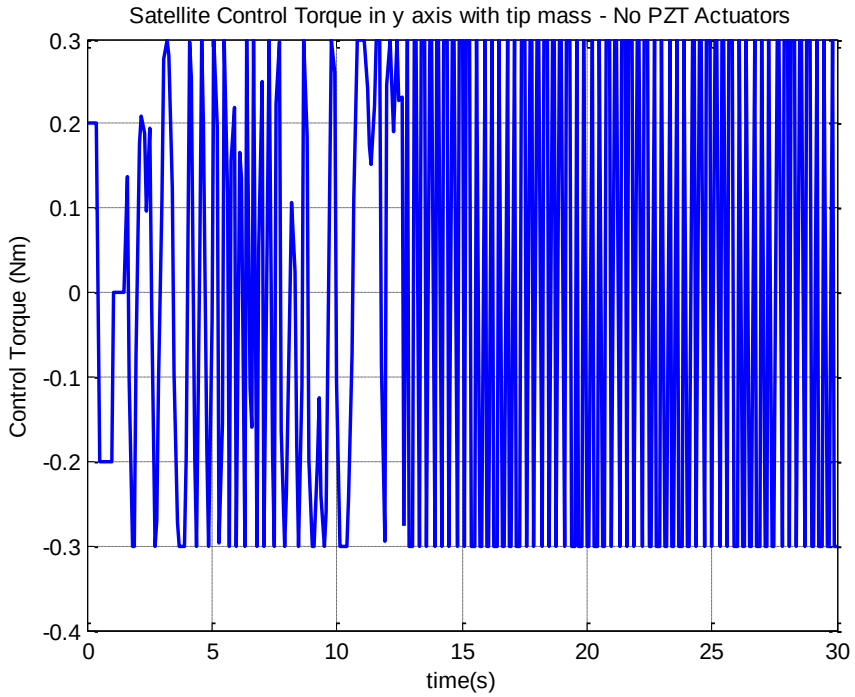

Figure 3.11: The disturbance torque (first 1 s) and control torque in y direction applied to the satellite with a tip mass - no PZT actuators

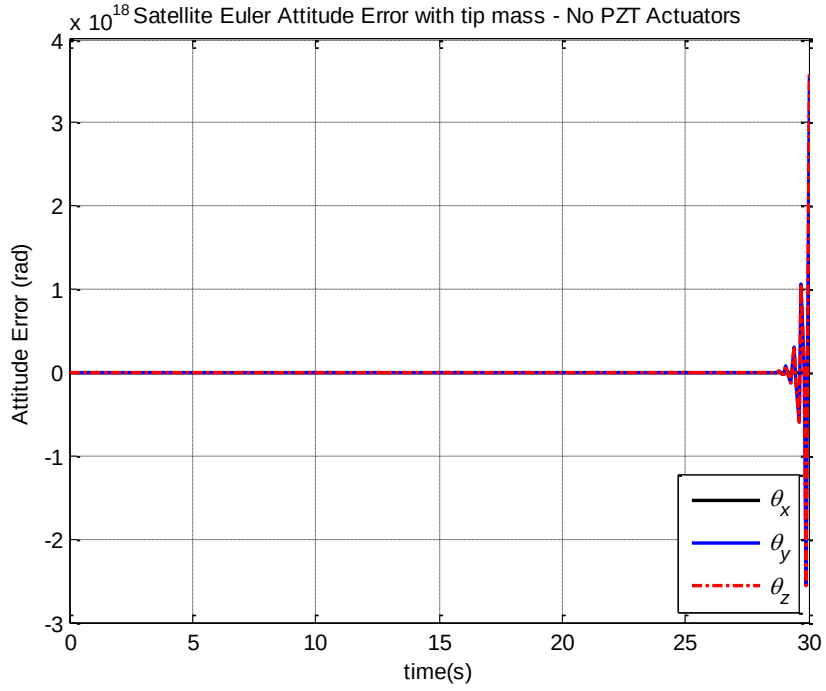

Figure 3.12: Satellite Euler attitude error with a tip mass - no PZT actuators

Table 3.3: Satellite accuracy, jitter and stability results (3σ) in 3 axes with a tip mass when there are no PZT actuators – 0.2 Nm torque input

	Accuracy Metric (°) *10^{19}	**Jitter Metric (°/s) *10^{19}**	**Stability Metric (°) *10^{20}**
x	0	0	0
y	7.8477	4.5400	1.1098
z	7.8477	4.5400	1.1098

This time the saturation of actuators leads an unstable as shown in Figure 3.12. The high actuator activity is also observable from Figure 3.11.

When 0.1 Nm disturbance torque input is applied, saturation of the actuators is no longer a problem as may be observed from Figure 3.13. The pointing performance is quite good (Figure 3.14 and Table 3.4). However, rapid and never dying actuator motion is evident in Figure 3.13.

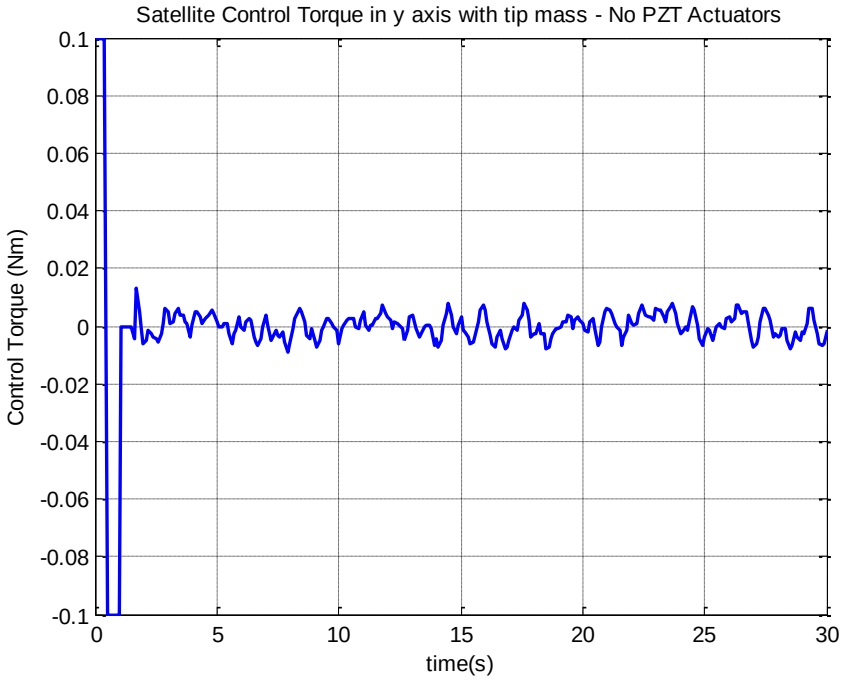

Figure 3.13: The disturbance torque (first 1 s) and control torque in y direction applied to the satellite with a tip mass - no PZT actuators

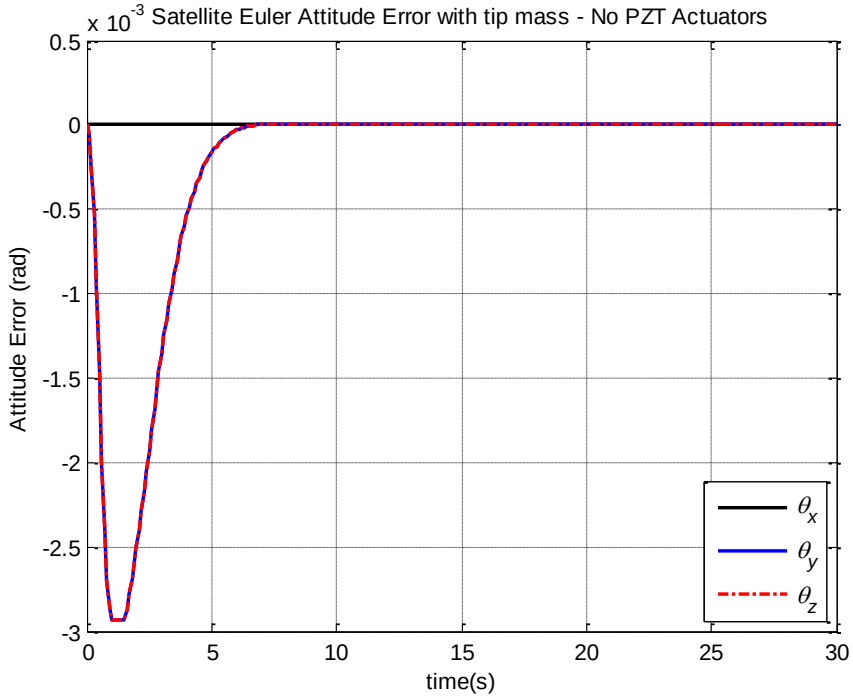

Figure 3.14: Satellite Euler attitude error with a tip mass - no PZT actuators

Table 3.4: Satellite accuracy, jitter and stability results (3σ) in 3 axes with a tip mass when there are no PZT actuators – 0.1 Nm torque input

	Accuracy Metric (°) *10^{-5}	**Jitter Metric (°/s) *10^{-6}**	**Stability Metric (°) *10^{-5}**
x	0	0	0
y	0.2141	0.1996	0.3536
z	0.2141	0.1996	0.3536

3.2.3. Case Study 3: Feedback Control without a Tip Mass (There is PZT Actuator Control)

In the case of applying the PZT actuator control, due to voltage limitations of the piezoelectric materials, two saturation blocks are added to the simulation model as shown in Figure 3.1. ±100 voltage limit on PZT actuator corresponds to 1.9132×10^{-2} Nm control torque limit (Eqn. (2.31)).

a. Low Level Satellite Disturbance Torque Input

When 0.1 Nm satellite disturbance torque input (Figure 3.8) is applied to the system, the response of the system is evaluated and discussed through simulation results in the following.

The nominal values of Q and R matrices used in all the simulations are as follows:

Q Matrix in M-File Code:

```
Q = 1e6*diag([1/(0.0001^2);
1/(0.00001^2);1/(0.001^2);1/(0.00001)^2;1/(0.001)^2;1/(0.00001)^2;
...
    1/(0.001)^2;1/(0.00001^2);1/(0.001^2);...
```

```
    1/(0.0001^2);
1/(0.00001^2);1/(0.001^2);1/(0.00001)^2;1/(0.001)^2;1/(0.00001)^2;
...
    1/(0.001)^2;1/(0.00001^2);1/(0.001^2);...

    1/(0.0001^2);
1/(0.00001^2);1/(0.001^2);1/(0.00001)^2;1/(0.001)^2;1/(0.00001)^2;
...
    1/(0.001)^2;1/(0.00001^2);1/(0.001^2);...
    1/(0.0001^2);
1/(0.00001^2);1/(0.001^2);1/(0.00001)^2;1/(0.001)^2;1/(0.00001)^2;
...
    1/(0.001)^2;1/(0.00001^2);1/(0.001^2)]) ;  % [36x36]
```

Nominal R matrix:

```
R = 1e12*eye(10) ;    % [10x10]
```

To design the weighting matrices (Q and R) of LQR control algorithm, numbers of simulations are carried out. In order to tune diagonal Q matrix, more weight is put on the satellite states which correspond to attitude errors in y and z axes. The system response to disturbance torque level 0.1 Nm is simulated and presented in the following figures.

It may be observed from Figure 3.15 and 3.16 that the attitude error rapidly decays. The reaction wheel as well as PZT activity also disappears as the spacecraft is brought to a steady pointing with very accurate pointing performance as given in Table 3.5.

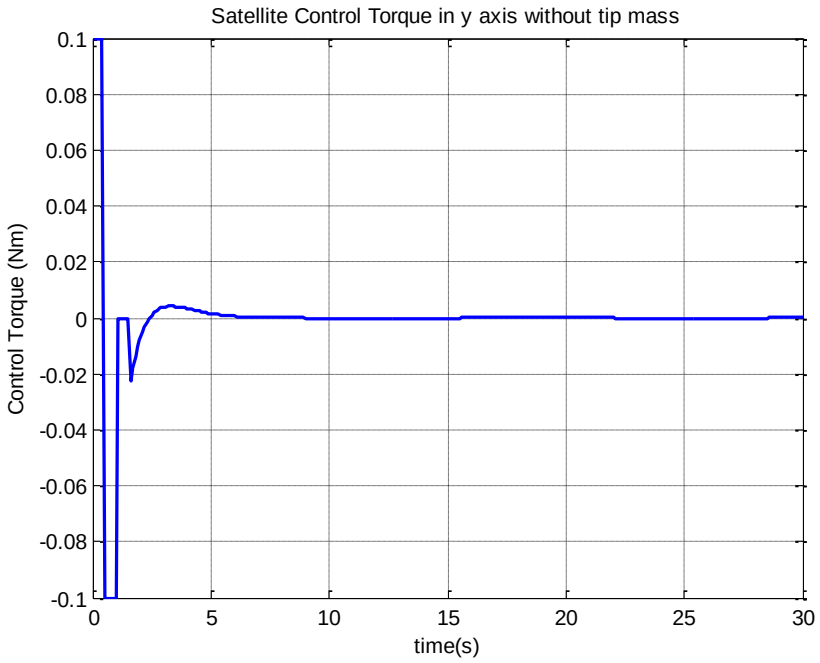

Figure 3.15: The disturbance torque (first 1 s) and control torque in y direction applied to the satellite without a tip mass

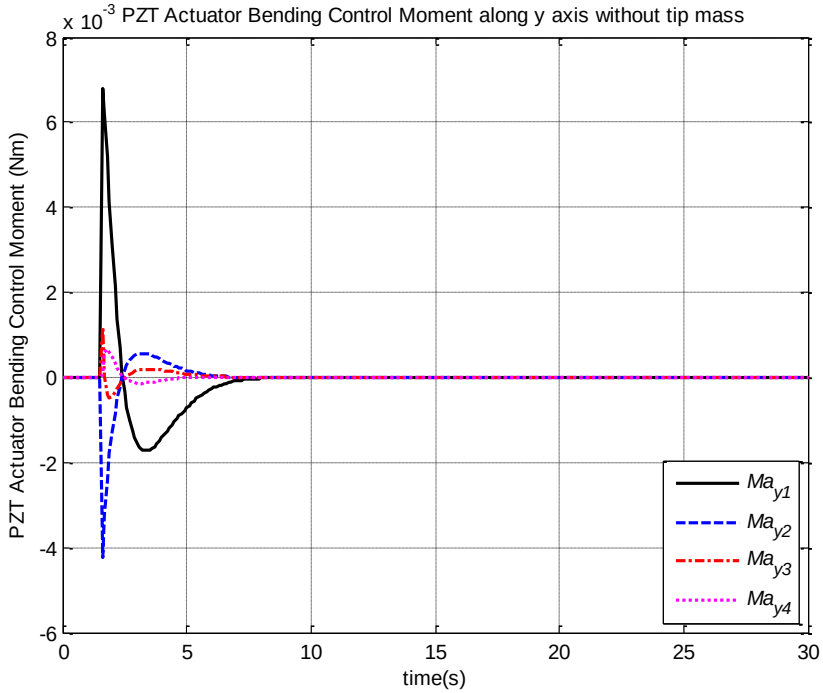

Figure 3.16: PZT actuator generated bending moments along y axis without a tip mass

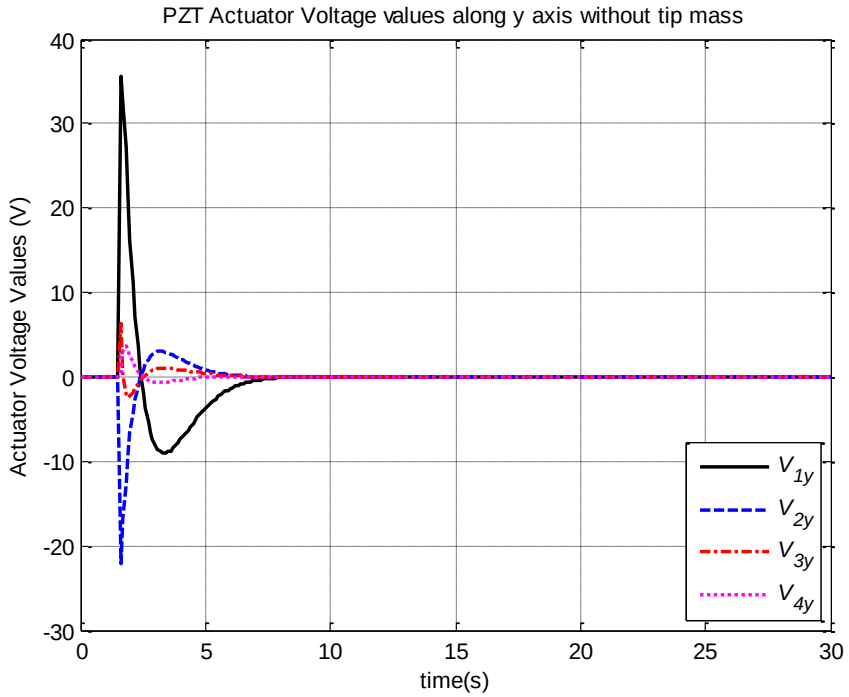

Figure 3.17: Y-direction PZT actuator voltages - without a tip mass

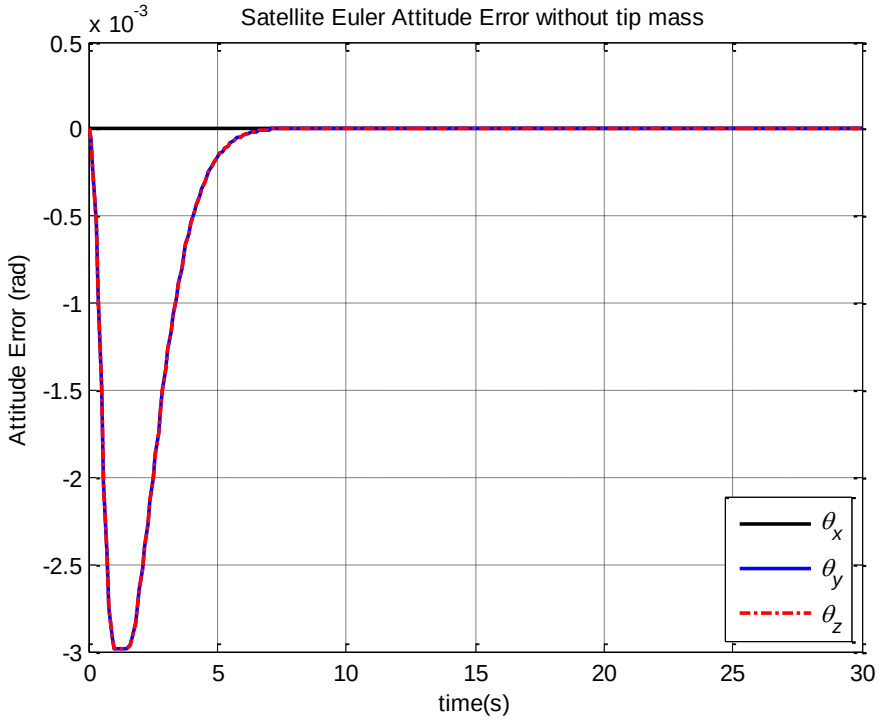

Figure 3.18: Satellite Euler attitude error without a tip mass

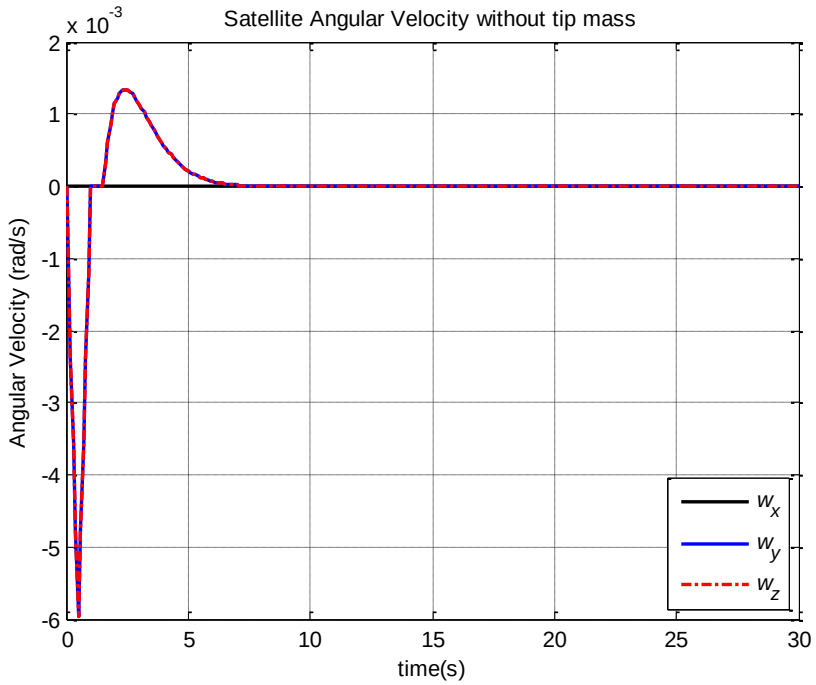

Figure 3.19: Satellite angular velocity without a tip mass

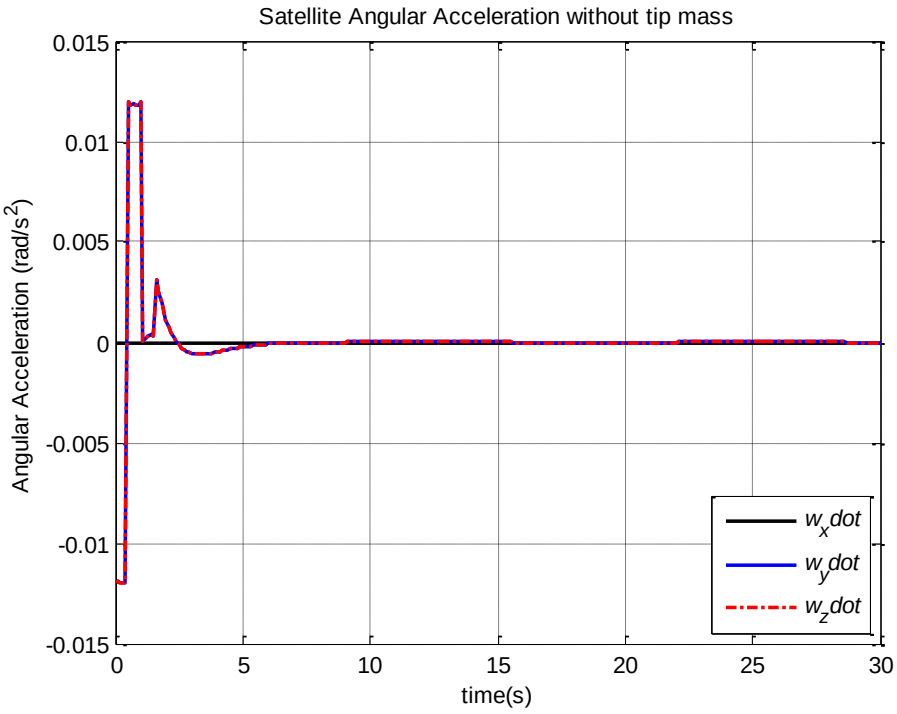

Figure 3.20: Satellite angular acceleration without a tip mass

Table 3.5: Satellite accuracy, jitter and stability results (3σ) in 3 axes without a tip mass when low level disturbance torque input is applied

	Accuracy Metric (°) *10^{-9}	**Jitter Metric (°/s) *10^{-10}**	**Stability Metric (°) *10^{-9}**
x	0	0	0
y	0.2360	0.2674	0.3217
z	0.2360	0.2674	0.3217

b. High Level Disturbance Torque

The simulations are carried out using high disturbance torque (0.2 Nm) as shown in Figure 3.5. The results are presented in figures 3.21-3.26.

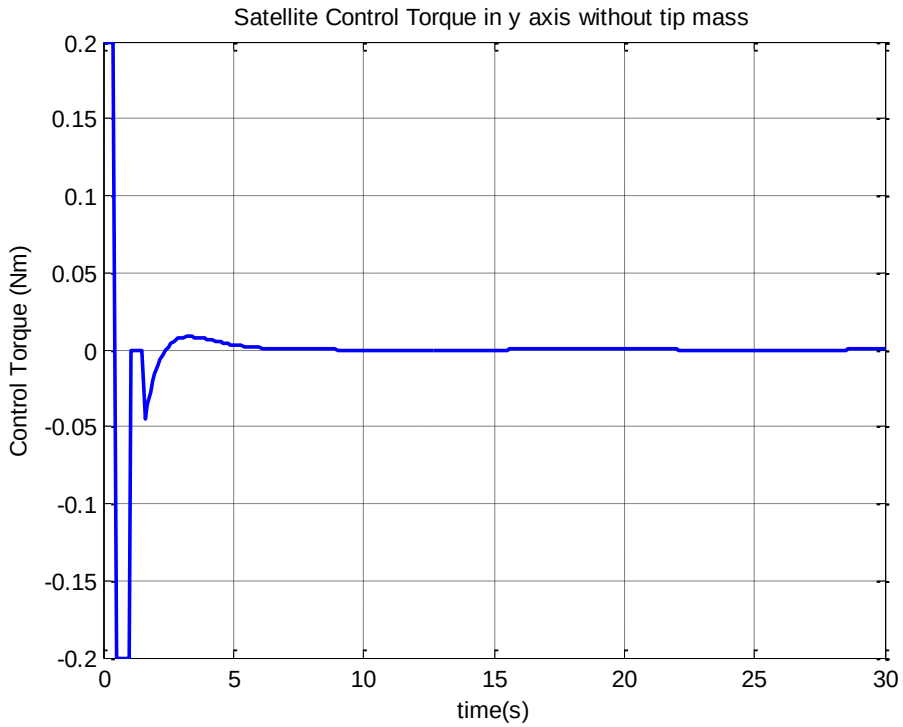

Figure 3.21: The disturbance torque (first 1 s) and control torque in y direction applied to the satellite without a tip mass

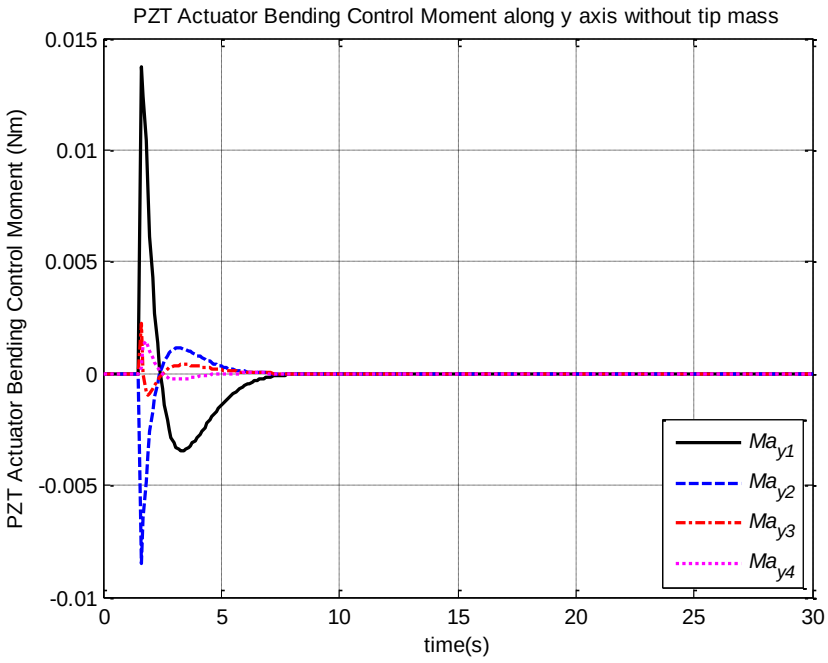

Figure 3.22: PZT actuator generated bending moments along y axis without a tip mass

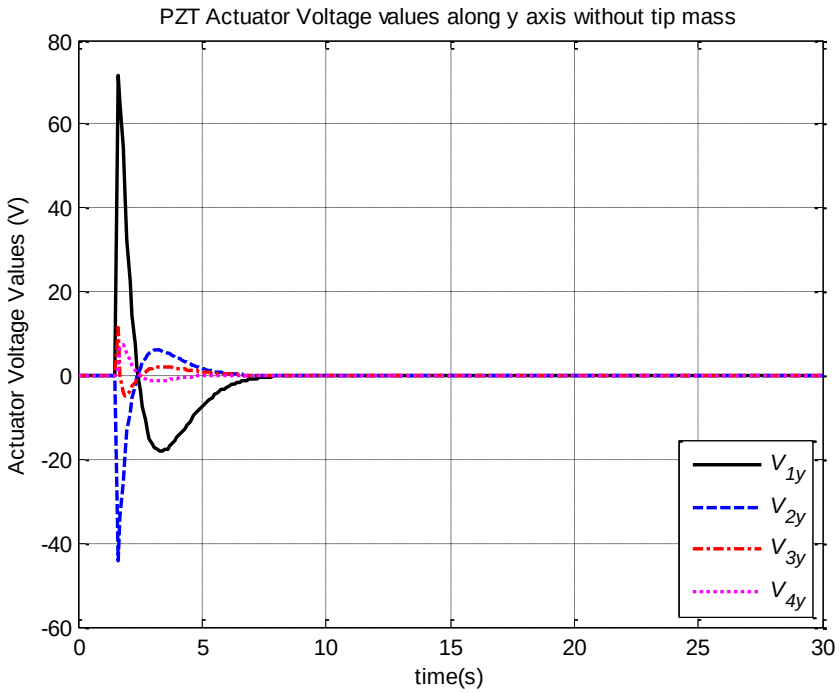

Figure 3.23: Y-direction PZT actuator voltages - without a tip mass

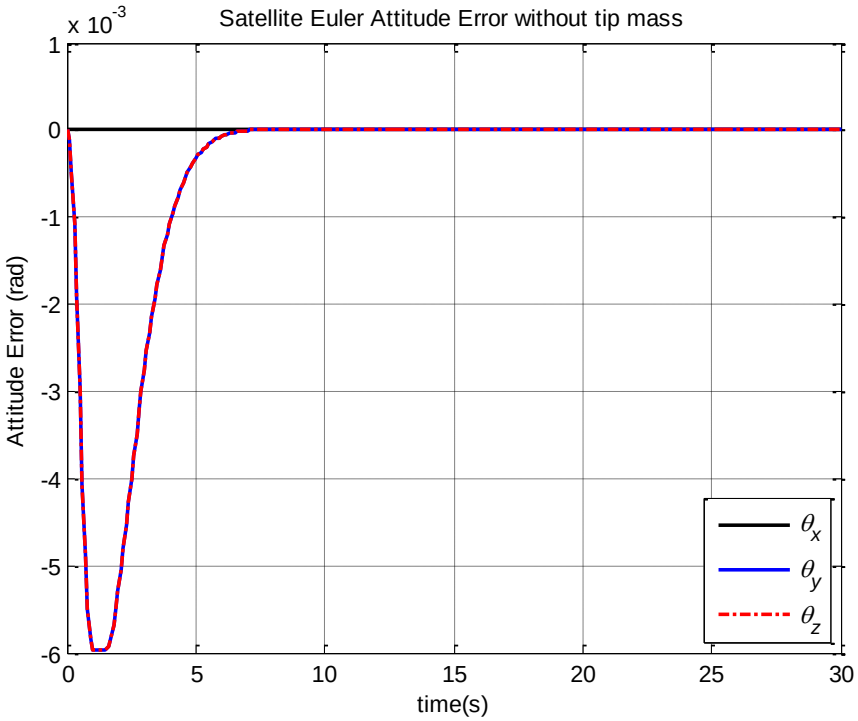

Figure 3.24: Satellite Euler attitude error without a tip mass

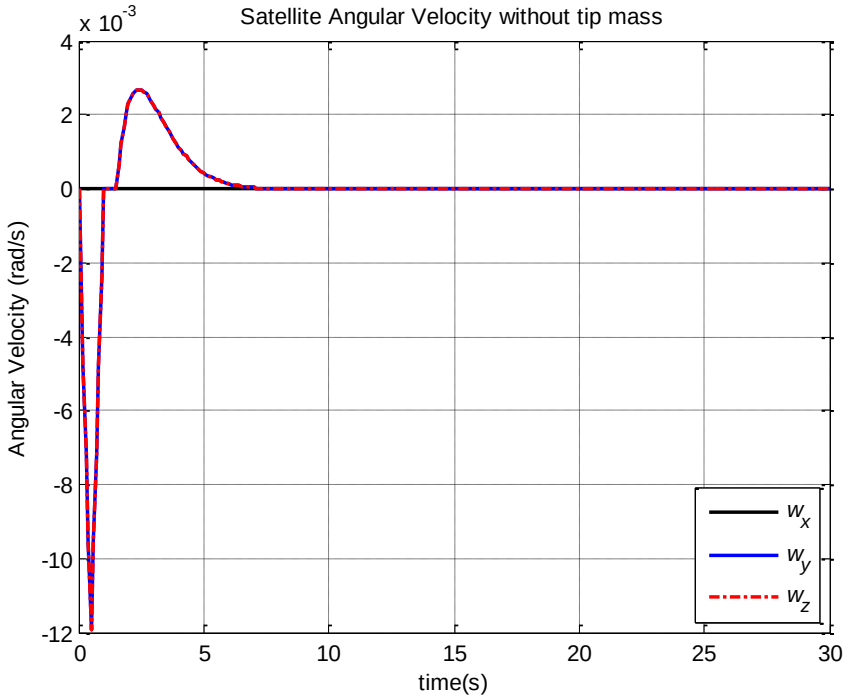

Figure 3.25: Satellite angular velocity without a tip mass

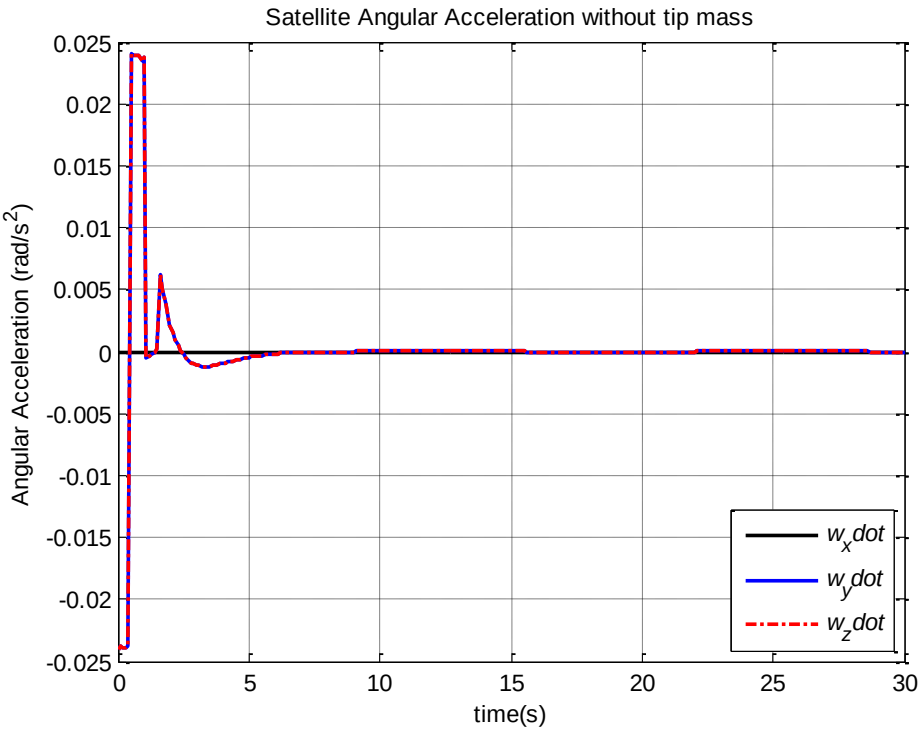

Figure 3.26: Satellite angular acceleration without a tip mass

Table 3.6: Satellite accuracy, jitter and stability results (3σ) in 3 axes without a tip mass when high level disturbance torque input is applied

	Accuracy Metric (°) *10^{-9}	**Jitter Metric (°/s) *10^{-10}**	**Stability Metric (°) *10^{-9}**
x	0	0	0
y	0.4720	0.5345	0.6434
z	0.4720	0.5345	0.6434

The satellite is again rapidly brought to steady pointing as before (Figures 3.24-3.26). The pointing performance is also excellent as may be observed from Table 3.6. Actuator activities are also low level and end quite rapidly as may be observed from Figure 3.21 and 3.22.

Comparing the results of “Low Level Disturbance Torque Input” case to the results of “High Level Disturbance Torque Input” case study, it may be concluded that the magnitudes of the outputs (control torques, voltages, satellite angular velocity, angular acceleration, pointing accuracy etc.) are directly proportional to the magnitudes of the disturbance acting on the system, since the system model is linear.

3.2.4. Case Study 4: Feedback Control with a Tip Mass (There is PZT Actuator Control)

a. Low Level Disturbance Torque Input

When the tip mass is included in the model and 0.1 Nm torque input is applied, the system response is evaluated though simulations and results are given in the following figures and tables.

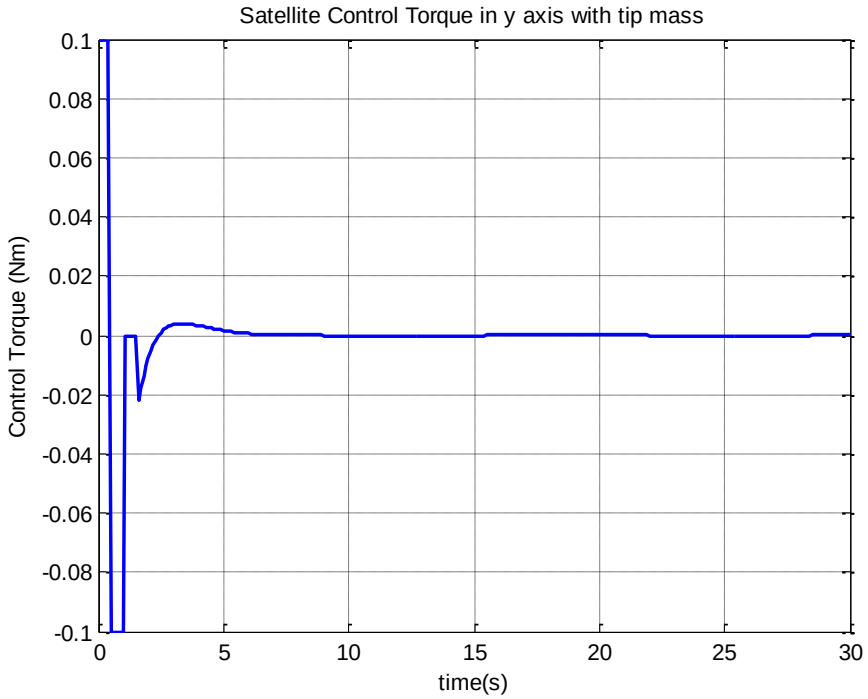

Figure 3.27: The disturbance torque (first 1 s) and control torque in y direction applied to the satellite with a tip mass

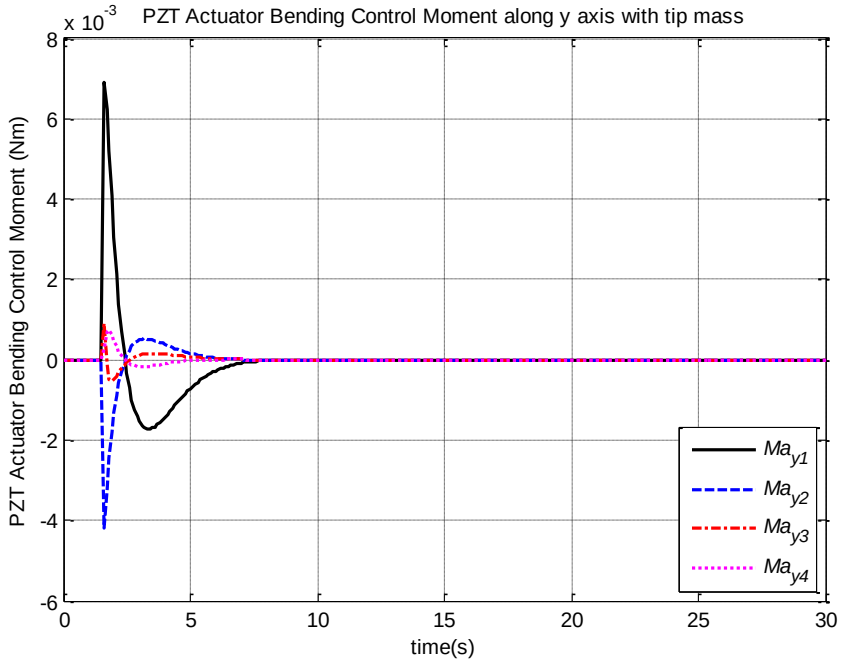

Figure 3.28: PZT actuator generated bending moments along y axis with a tip mass

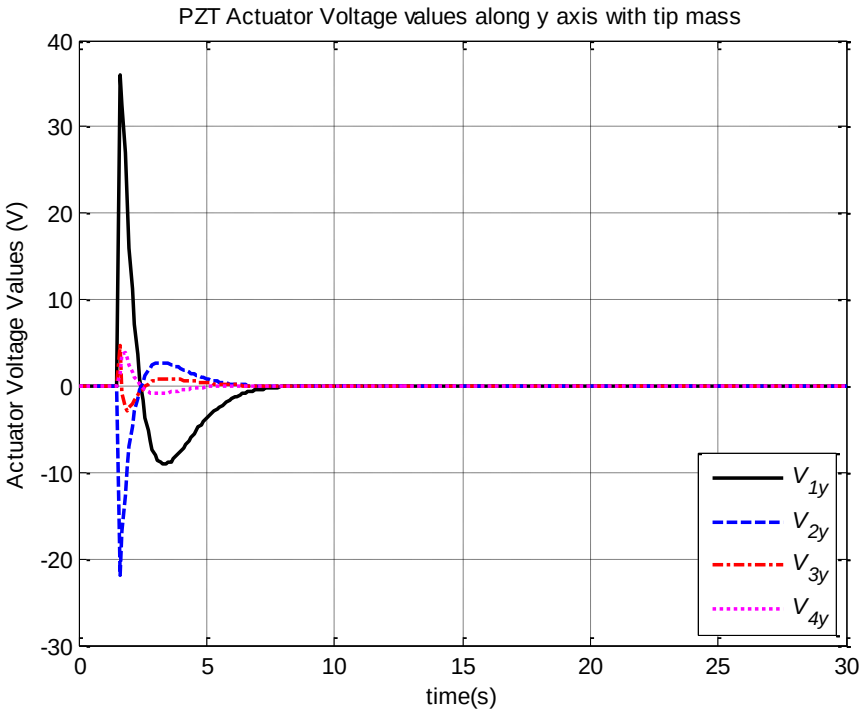

Figure 3.29: Y-direction PZT actuator voltages - with a tip mass

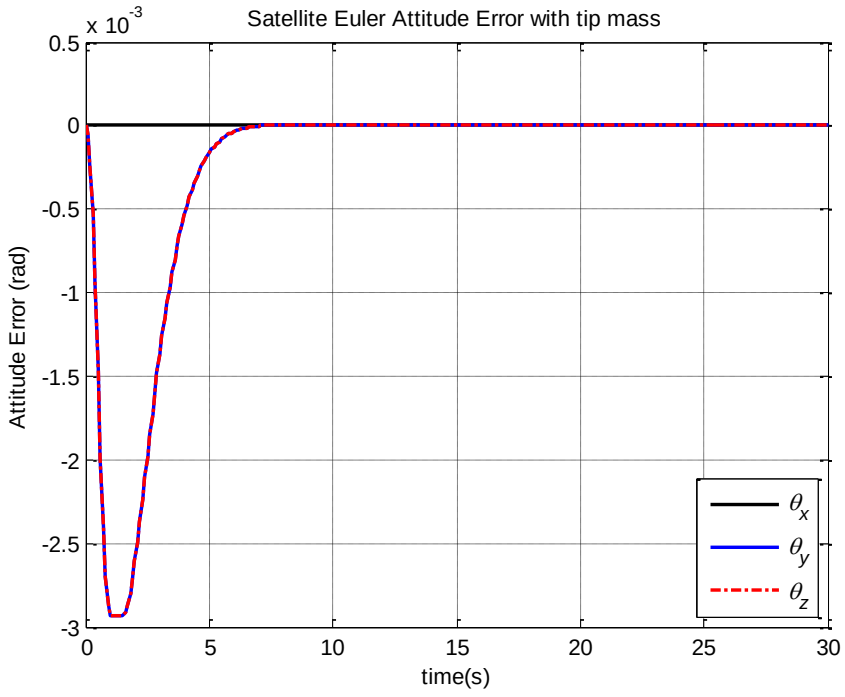

Figure 3.30: Satellite Euler attitude error with a tip mass

As may be observed from these figures, rapid and accurate attitude control is achieved when PZT actuators are working together with the reaction wheels on the satellite body.

Table 3.7: Satellite accuracy, jitter and stability results (3σ) in 3 axes with a tip mass when low level disturbance torque input is applied

	Accuracy Metric (°) *10^{-9}	**Jitter Metric (°/s) *10^{-10}**	**Stability Metric (°) *10^{-9}**
x	0	0	0
y	0.3174	0.2185	0.4208
z	0.3174	0.2185	0.4208

The satellite accuracy and the stability metrics results in 3.2.3.a case study without the tip mass are better than these results when Table 3.5 and Table 3.7 are compared. However, the jitter metric value is much better in this case.

b. High Level Disturbance Torque Input

In this case study, 0.2 Nm torque input is used to run the simulation model with the tip mass.

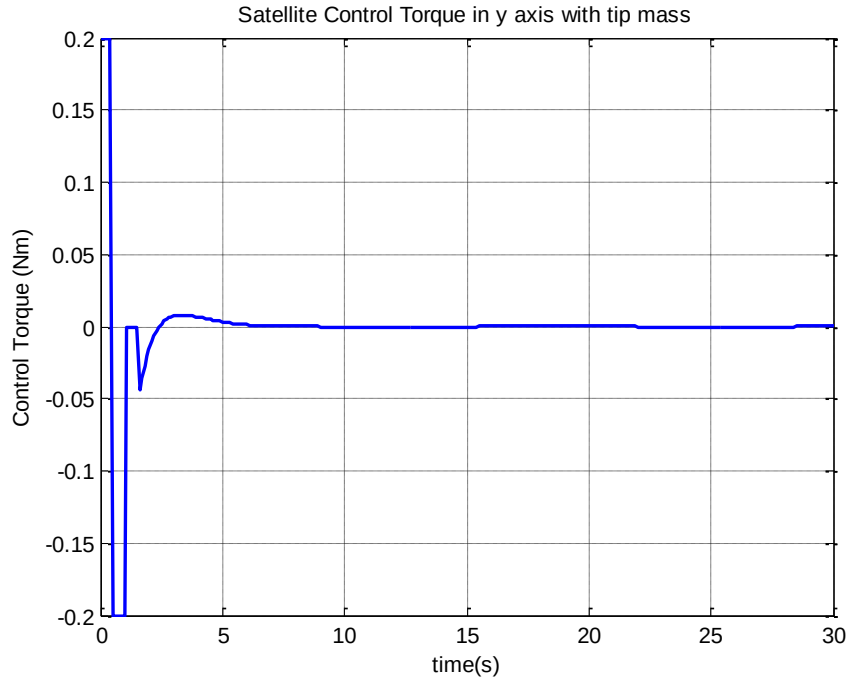

Figure 3.31: The disturbance torque (first 1 s) and control torque in y direction applied to the satellite with a tip mass

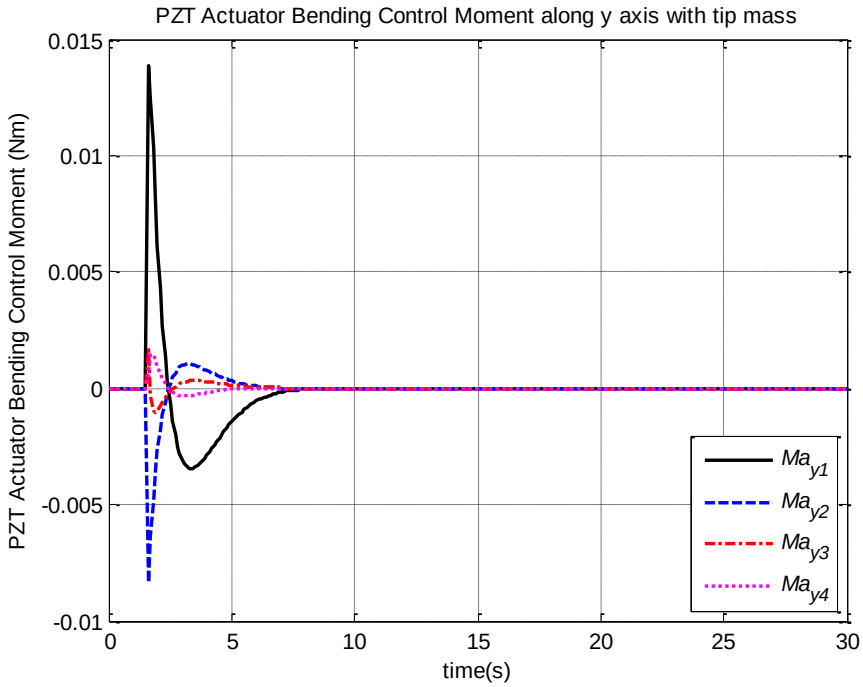

Figure 3.32: PZT actuator generated bending moments along y axis with a tip mass

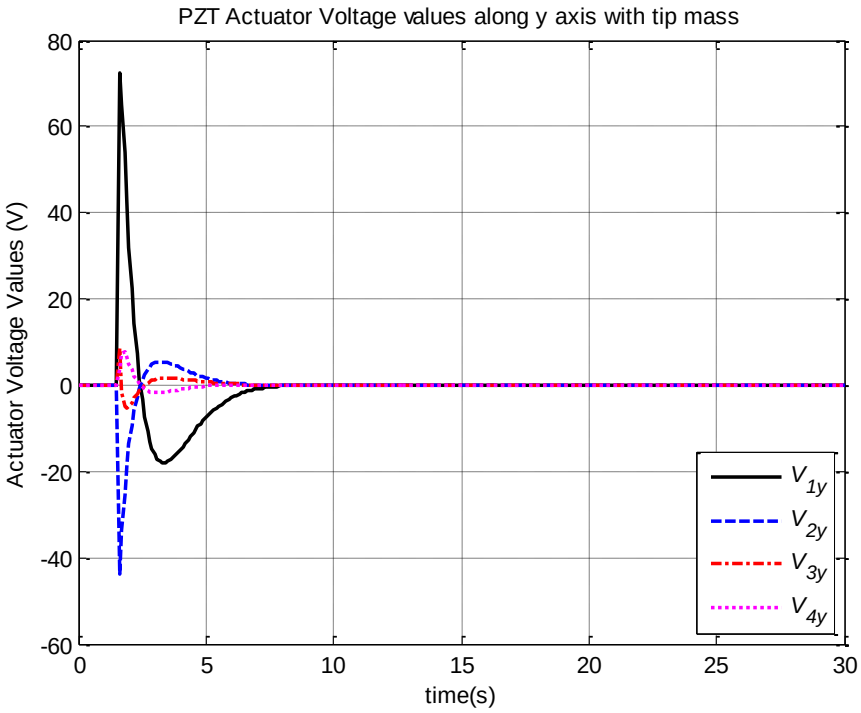

Figure 3.33: Y-direction PZT actuator voltages - with a tip mass

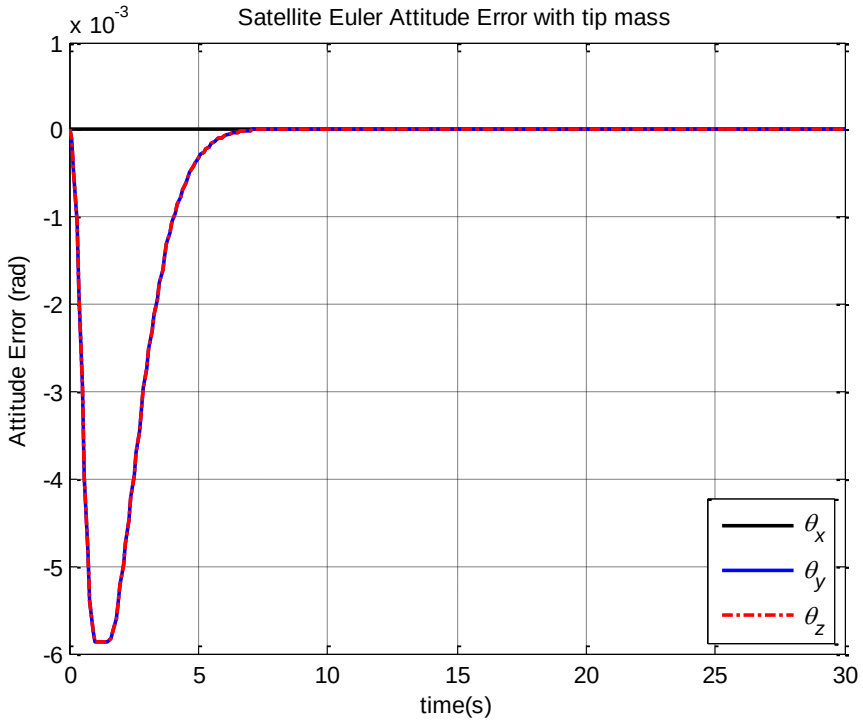

Figure 3.34: Satellite Euler attitude error with a tip mass

Table 3.8: Satellite accuracy, jitter and stability results (3σ) in 3 axes with a tip mass when high level disturbance torque input is applied

	Accuracy Metric (°) *10^{-9}	**Jitter Metric (°/s) *10^{-10}**	**Stability Metric (°) *10^{-9}**
x	0	0	0
y	0.6346	0.4356	0.8412
z	0.6346	0.4356	0.8412

Comparing these results to the (3.2.3.b) case simulation results, it may be concluded that including the tip mass while PZT actuator control is available effective and rapid system control with excellent pointing performance is achieved.

CHAPTER 4

SUMMARY AND CONCLUSION

4.1. Summary

In this thesis, an attitude control system based on LQR control method was developed to improve the pointing performance of a hypothetical observation satellite with a flexible smart beam with piezoelectric actuators. The rectangular beam was modeled together with piezoelectric layers bonded on all four surfaces using finite element method and considering classical Euler-Bernoulli beam assumption.

The numerous simulation studies for different cases depending on the tip mass, PZT actuator control and disturbance torque input levels are carried out. The simulation results are compared and discussed. Using satellite attitude error simulation results, the satellite pointing performance results were calculated and discussed for each simulation case study.

4.2. Conclusion

Based on the simulation results carried out for various case studies, it is shown that inclusion of PZT actuators significantly reduces satellite actuator activity. The required torque levels from reaction wheels also drop significantly below

saturation levels. Properly selected different weighting matrices lead to better satellite pointing performance.

4.3. Suggestions for Future Work

The following may be recommended for future study:

- In addition to the LQR control method, different control approaches should be investigated to improve the pointing performance of the satellite with flexible boom

- The disturbance due to the unbalance forces of the Reaction Wheels operated in a satellite and effects of slew maneuver as a disturbance shall also be considered. In addition, the propellant sloshing effects during a slew maneuver may be taken into account

- Implementation of control with PZT actuators shall also be tested experimentally and hopefully in orbit.

REFERENCES

[1] B. Agraval, “Jitter Control for Imaging Spacecraft”, Department of Mechanical and Astronautical Engineering Naval Postgraduate School, USA, Recent Advances in Space Technologies (RAST) 4th International Conference, 2009

[2] W. Keith Belvin, “Spacecraft Jitter Attenuation Using Embedded Piezoelectric Actuators”, NASA Langley Research Center publication, 1995

[3] http://www.eoportal.org/directory/pres_RADARSAT1.html (last accessed September 12, 2011)

[4] https://directory.eoportal.org/get_announce.php?an_id=7357 (last accessed September 12, 2011)

[5] http://www.eoportal.org/directory/pres_GeoEye1OrbView5.html (last accessed September 12, 2011)

[6] http://www.eoportal.org/directory/pres_EO1EarthObserving1.html (last accessed September 12, 2011)

[7] http://www.dlr.de/eo/en/desktopdefault.aspx/tabid-5725/9296_read-15979/ (last accessed September 12, 2011)

[8] E. H. Anderson, J. P. How, "Adaptive feedforward control for actively isolated spacecraft platforms", AIAA/ASME/ASCE/AHS/ASC Structures, Structural Dynamics, and Materials Conference and Exhibit, Kissimmee, FL, April 1997 (AIAA-97-1200)

[9] S. Kayastha, O. Tekinalp, and K. Ozgoren, “Pointing performance control of a spacecraft camera using piezoelectric actuators”, "20th AAS/AIAA Space Flight Mechanics Meeting, San Diego, CA, Feb. 14-17 2010."

[10] S. Narayanan, V. Balamurugan, “Finite Element Modelling of Piezolaminated Smart Structures for Active Vibration Control with Distributed Sensors and Actuators”, Journal of Sound and Vibration, 262 (2003 529-562)

[11] C. M. A. Vasques, J. D. Rodrigues, "Active Vibration Control of Smart Piezoelectric Beams: Comparison of Classical and Optimal Feedback Control Strategies", Computers and Structures 84 (2006) 1402–1414

[12] L. Malgaca, Integration of Active Vibration Control Methods With Finite Element Models of Smart Structures, PhD Thesis, Mechanical Engineering Department, Dokuz Eylül University Libraries, May 2007

[13] B. Bandyopadhyay, T. C. Manjunath, M. Umapathy, Modeling, Control and Implementation of Smart Structures, Springer, Berlin, 2007

[14] C. M. de A. Vasques, Vibration Control of Adaptive Structures, Modeling, Simulation and Implementation of Viscoelastic and Piezoelectric Damping Technologies, PhD Thesis, University of Porto, 2008

[15] M. Moshrefi-Torbati, A.J. Keane, S.J. Elliott, M.J. Brennan, D.K. Anthony, E. Rogers, "Active vibration control (AVC) of a satellite boom structure using optimally positioned stacked piezoelectric actuators", Journal of Sound and Vibration, 2002

[16] A. Zabihollah, R. Sedagahti and R. Ganesan, "Active vibration suppression of smart laminated beams using layerwise theory and an optimal control strategy", Smart Materials and Structures 16 (2007) 2190–2201

[17] H. Irschik, M. Krommer, Y. Vetyukov, "On the use of piezoelectric sensors in structural mechanics: Some novel strategies", ISSN 1424-8220, Sensors 2010

[18] D. S. Stampleman, Active microgravity vibration isolation using PVDF polymer piezoelectric actuators, Master's Thesis, Massachusetts Institute of Technology, 1991

[19] http://www.piceramic.com/piezo_tutorial1.php (last accessed September 12, 2011)

[20] M. B. Basem, G. A. Wahied, "Nanopositioning Fuzzy Control for Piezoelectric Actuators", International Journal of Engineering &Technology IJET-IJENS Vol: 10 No: 01

[21] D. R. Fay, "Vibration Control in a Smart Beam", AIAA Regional Student Conference, Baltimore, Maryland, April 2003

[22] P. Gaudenzi, Smart Structures Physical Behaviour, Mathematical Modelling and Applications, University of Roma, Italy, 2009, Wiley

[23] Q. Hu, G. Ma "Variable structure control and active vibration suppression of flexible spacecraft during attitude maneuver", Aerospace Science and Technology 9 (2005) 307–317

[24] J. L. Junkins, Y. Kim, Introduction to Dynamics and Control of Flexible Structures, AIAA Education Series, Ohio, Second Printing 1993

[25] P. S. King, Linear State Feedback Controller Design, National University of Singapore, October 17, 2010

[26] B. Wie, Space Vehicle Dynamics and Control, AIAA Education Series, Ohio, 1998

[27] J. P. Hespanha, Undergraduate Lecture Notes on LQG/LQR controller design, April 2007

[28] M. E. Pittelkau, "Definitions, Metrics, and Algorithms for Displacement, Jitter, and Stability", NASA/CP-2003-212246

[29] A.Y. Lee, J. W. Yu, P. B. Kahn, R. L. Stoller, "Space Interferometry Mission Spacecraft Pointing Error Budgets", Jet Propulsion Laboratory, IEEE Transactions on Aerospace and Electronic Systems Vol. 38, No. 2 April 2002